Functional impact of an oculopharyngeal muscular dystrophy mutation in PABPN1

Maricela García-Castañeda[1], Ana Victoria Vega[3], Rocío Rodríguez[2], Maria Guadalupe Montiel-Jaen[1], Bulmaro Cisneros[2], Angel Zarain-Herzberg[4] and Guillermo Avila[1] (iD)

[1] *Department of Biochemistry, Cinvestav-IPN AP 14-740, México City, México*
[2] *Department of Molecular Biology, Cinvestav-IPN AP 14-740, México City, México*
[3] *UBIMED FES-Iztacala, National Autonomous University of Mexico, Mexico City, México*
[4] *Department of Biochemistry, School of Medicine, National Autonomous University of Mexico, Mexico City, México*

Key points

- Mutations in the gene encoding poly(A)-binding protein nuclear 1 (PABPN1) result in oculopharyngeal muscular dystrophy (OPMD). This disease is of late-onset, but the underlying mechanism is unclear.
- Ca^{2+} stimulates muscle growth and contraction and, because OPMD courses with muscle atrophy and weakness, we hypothesized that the homeostasis of Ca^{2+} is altered in this disorder.
- C2C12 myotubes were transfected with cDNAs encoding either PABPN1 or the PABPN1-17A OPMD mutation. Subsequently, they were investigated concerning not only excitation–contraction coupling (ECC) and intracellular levels of Ca^{2+}, but also differentiation stage and nuclear structure.
- PABPN1-17A gave rise to: inhibition of Ca^{2+} release during ECC, depletion of sarcoplasmic reticulum Ca^{2+} content, reduced expression of ryanodine receptors, altered nuclear morphology and incapability to stimulate myoblast fusion.
- PABPN1-17A failed to inhibit ECC in adult muscle fibres, suggesting that its effects are primarily related to muscle regeneration.

Abstract   Oculopharyngeal muscular dystrophy (OPMD) is linked to mutations in the gene encoding poly(A)-binding protein nuclear 1 (PABPN1). OPMD mutations consist of an expansion of a tract that contains 10 alanines (to 12–17). This disease courses with muscle weakness that begins in adulthood, but the underlying mechanism is unclear. In the present study, we investigated the functional effects of PABPN1 and an OPMD mutation (PABPN1-17A) using myotubes transfected with cDNAs encoding these proteins (GFP-tagged). PABPN1 stimulated myoblast fusion (100%), whereas PABPN1-17A failed to mimic this effect. Additionally, the OPMD mutation markedly altered nuclear morphology; specifically, it led to nuclei with a more convoluted and ovoid shape. Although PABPN1 and PABPN1-17A modified the expression of sarcoplasmic/endoplasmic reticulum Ca^{2+}-ATPase and calsequestrin, the corresponding changes did not have a clear impact on $[Ca^{2+}]$. Interestingly, neither L-type Ca^{2+} channels, nor voltage-gated sarcoplasmic reticulum (SR) Ca^{2+} release (VGCR) was altered by PABPN1. However, PABPN1-17A produced a selective inhibition of VGCR (50%). This effect probably arises from both lower expression of RyR1 and depletion of SR Ca^{2+}. The latter, however, was not related to inhibition of store-operated Ca^{2+} entry. Both PABPN1 constructs promoted a moderated decrease in cytosolic $[Ca^{2+}]$, which apparently results from down-regulation of excitation-coupled Ca^{2+} entry. On the other hand, PABPN1-17A did not alter ECC in muscle fibres, suggesting that adult muscle is less prone to developing deleterious effects. These results demonstrate that PABPN1 proteins regulate essential processes during myotube formation and support the notion that OPMD involves disruption of myogenesis, nuclear structure and homeostasis of Ca^{2+}.

Abbreviations   CSQ, calsequestrin; DMEM, Dulbecco's modified Eagle's medium; DHPRs, dihydropyridine receptors; DM1, myotonic dystrophy type 1; ECC, excitation–contraction coupling; ECCE, excitation-coupled Ca²⁺ entry; FDB, flexor digitorum brevis; INI, intranuclear inclusion; L-channels, L-type Ca²⁺ channels; OPMD, oculopharyngeal muscular dystrophy; PABPN1, poly(A)-binding protein nuclear 1; PLB, phospholamban; RyR1s, ryanodine receptors; RT, room temperature; SERCA, sarcoplasmic/endoplasmic reticulum Ca²⁺ ATPase; SOCE, store-operated Ca²⁺ entry; SR, sarcoplasmic reticulum; VGCR, voltage-gated sarcoplasmic reticulum Ca²⁺ release.

Introduction

The couplonopathies are diseases of striated muscle that share a substantial disruption of the functional unit of Ca^{2+} release for excitation–contraction coupling (ECC), the couplon (Ríos *et al.* 2015). In skeletal muscle, ECC depends on a physical interaction between dihydropyridine receptors (DHPRs) and ryanodine receptors (RyR1s). The former are voltage-dependent L-type Ca^{2+} channels (L-channels), whereas the latter function as intracellular Ca^{2+} release channels. In response to membrane depolarization, the DHPRs are assumed to undergo conformational changes that open the RyR1s and thereby result in sarcoplasmic reticulum (SR) Ca^{2+} release. The resulting rise in cytoplasmic Ca^{2+} activates both the contractile machinery and the sarcoplasmic/endoplasmic reticulum Ca^{2+} ATPase (SERCA) that pumps Ca^{2+} back up into the SR (Melzer *et al.* 1995; Dirksen, 2002; Rebbeck *et al.* 2014).

Oculopharyngeal muscular dystrophy (OPMD) is a congenital myopathy that manifests in the fourth to sixth decades of life. It is characterized by dysphagia, ptosis, dysphonia, atrophy and proximal limb weakness. OPMD is caused by expansions of the GCG (alanine) trinucleotide repeat in the coding sequence of the poly(A)-binding protein nuclear 1 (PABPN1) gene (Brais *et al.* 1998). PABPN1 is a nuclear protein whose canonical role is to bind to nascent poly(A) tails of mRNA, enhancing the mRNA extension and controlling the respective size. In its N-terminus, PABPN1 presents a GCG trinucleotide repeat encoding for a tract of 10 alanines, which is expanded in OPMD mutations (to 12–17). OPMD is a polyalanine trinucleotide (GCG) repeat disease that shares common features with other polyglutamine (CAG) disorders, including Huntington's disease, as well as with other polyalanine and dystrophic disorders (Abu-Baker & Rouleau, 2006; Messaed & Rouleau, 2009; Banerjee *et al.* 2013).

Presumably, as a result of the polyalanine expansion, the mutant proteins aggregate into intranuclear inclusions (INIs), which sequester poly(A) RNA, ubiquitin, and subunits of the proteasome (Calado *et al.* 2000; Abu-Baker *et al.* 2003). This aggregation is considered to be toxic and cause cell death (Fan *et al.* 2001), which may explain the symptoms in OPMD (Davies *et al.* 2005; Davies *et al.* 2006). However, the observation that INIs are observed in only a small fraction of muscle nuclei (<0.1) (Blumen *et al.* 1999) suggests that these abnormalities are probbaly not the only pathophysiological mechanism. Accordingly, evidence exists indicating that the polyalanine tract is not essential for the aggregation of PABPN1 (Fan *et al.* 2001; Tavanez *et al.* 2005).

During the skeletal muscle development (myogenesis), precursor cells (myoblasts) withdraw from the cell cycle and fuse in a process termed terminal differentiation. The resulting cells, known as myotubes, gradually express the molecular elements that are involved in ECC. Myogenesis is of paramount relevance for muscle growth, maintenance and repair in response to injury (Beam & Franzini-Armstrong, 1997; Horsley & Pavlath, 2004; Benavides Damm & Egli, 2014). There is increasing evidence suggesting that PABPN1 is critical for stimulating myogenesis. For example, compared with their parent cells, stable lines of myoblasts that overexpress PABPN1 show both enhanced myotube formation and increased expression of myogenic factors (Kim *et al.* 2001). Conversely, the absence of PABPN1 not only reduces levels of myogenic factors and myotubes size, but also impairs myoblast proliferation (Apponi *et al.* 2010; Anvar *et al.* 2013). Moreover, alterations in muscle differentiation are considered to contribute to the pathophysiology of OMPD (Périé *et al.* 2006; Wang & Bag, 2006; Apponi *et al.* 2013). A precedent for this view is that myotubes expressing an OPMD mutation that encodes a PABPN1 with seven additional alanine residues (PABPN1-17A) exhibit low levels of the myogenic factors MyoD and myogenin. Apparently, this action is a result of down-regulation of Myf5 and Pax3/7, which control myogenesis upstream of the former factors (Wang & Bag, 2006). Accordingly, satellite cells from OPMD patients proliferate and fuse to a lesser extent than those from age-matched controls (Périé *et al.* 2006).

To date, no data exist concerning the homeostasis of Ca^{2+} in the context of either PABPN1 or OPMD, which is surprising given that this ion participates not only in force development and myogenesis, but also in several other biological processes (Melzer *et al.* 1995; Benavides Damm & Egli, 2014). Thus, the present study aimed to

assess the functional impact of two GFP-tagged PABPN1 constructs (wild-type and PABPN1-17A) with respect to not only ECC and homeostasis of Ca^{2+}, but also terminal differentiation and nuclear morphology. We found that these two proteins regulate essential processes during myotube formation. For example, the OPMD mutation gives rise to significant alterations in voltage-gated Ca^{2+} release (VGCR), SR Ca^{2+} content, nuclear structure and the ability of PABPN1 to stimulate myoblast fusion. These effects could represent fundamental alterations in muscle remodelling during OPMD progression.

Methods

Cell culture and plasmid constructs

The C2C12 cell line was acquired from the American Type Culture Collection (ATCC, Manassas, VA, USA). Cells were plated on 35 mm Petri dishes that contained proliferation medium, consisting of Dulbecco's modified Eagle's medium (DMEM) supplemented with 20% fetal bovine serum, penicillin ($100 \, U \, ml^{-1}$) and streptomycin ($100 \, \mu g \, ml^{-1}$). Myogenesis was induced by replacing proliferation medium with differentiation medium, which was identical to the former, but contained 2% horse serum instead of 20% fetal bovine serum. The cDNAs encoding human PABPN1 and PABPN1-17A were cloned into the pEGFP-C2 vector (Abu-Baker *et al.* 2003); thus, the respective products consist of EGFP-tagged proteins (EGFP-PABPN1 and EGFP-PABPN1-17A). For simplicity, they are referred to as PABPN1 and PABPN1-17A. The plasmids used as transfection control were: pDsRed-N1 and pEGFP-C1. Cells were transfected before differentiation with FuGENE® HD reagent (Promega, Madison, WI, USA) in accordance with the manufacturer's instructions. For this, 2 μg of plasmid cDNA per dish was added, and the transfected myotubes were identified by fluorescence microscopy (Vega *et al.* 2011). Experiments were performed after 5–8 days of differentiation.

In vivo transfection and isolation of adult muscle fibres

The flexor digitorum brevis (FDB) of adult Balb/c mice (6–8 weeks of age, unless otherwise specified) was transfected by electroporation *in vivo*, as described previously (Aihara & Miyazaki, 1998; DiFranco *et al.* 2009). This protocol was approved by the Institutional Animal Care and Use Committee (IAUCC – CINVESTAV, 0259-05), complies with the Mexican Official Norm NOM-062-ZOO-1999 and was designed in accordance with the Guide for the Care and Use of Laboratory Animals. Briefly, mice were anaesthetized by I.P. injection of ketamine ($100 \, mg \, kg^{-1}$), xylazine ($10 \, mg \, kg^{-1}$)

and acepromazine ($3 \, mg \, kg^{-1}$). The effectiveness of anaesthesia was corroborated by the absence of voluntary movements and stretch reflexes. Once anaesthetized, 10 μl of hyaluronidase was injected into the footpads, using a Hamilton syringe. Sixty minutes later, 35 μg of cDNA (encoding either EGFP-PABPN1 or EGFP- PABPN1-17A) was injected. The animal was again anaesthetized, before being impaled with two electrodes (just below the skin) and the muscles were electroporated by applying 20 pulses of 20 ms each, at 1 Hz ($\sim$100 Vcm^{-1} of an electric field).

Within 1 week to 5 months after the time of electro-poration, single FDB fibres were isolated in accordance with methods described previously (Anderson *et al.* 2012; Keire *et al.* 2013). The animals were killed by CO_2 inhalation, and the FDB was dissected from the hind limb. The muscle sample was placed in Ringer solution and transferred into a digesting solution consisting of DMEM added with EGTA (1.7 mM), Na-pyruvate (1 mM), penicillin ($100 \, UI \, ml^{-1}$), streptomycin ($100 \, \mu g \, ml^{-1}$) and collagenase IA ($2.0 \, mg \, ml^{-1}$). The sample was incubated (1 h at 37°C), transferred into a Ringer solution to which 25 mM creatine was added and gently dispersed with a Pasteur pipette. The isolated fibres were kept at 4°C and used for voltage clamp experiments within the next 8 h.

Immunofluorescence

C2C12 myotubes that grew on glass coverslips were fixed with 4% paraformaldehyde (15 min) and permeabilized by exposure to PBS-SDS. The slides were washed with PBS and blocked during 20 min using PBS added with 0.5% gelatin and 1.5% BSA at room temperature (RT). Subsequently, they were incubated overnight at 4°C with primary monoclonal antibody anti-SERCA2 (clone 2A7-A1; Sigma, St Louis, MO, USA). The cell preparations were washed three times with PBS and then incubated with anti-mouse IgG conjugated to Alexa 546 (1 h at RT). Nuclei were counterstained with Hoechst (0.2 μg μl^{-1} for 6 min at RT), and the samples were washed with PBS before being mounted with VectaShield (Vector Laboratories, Inc., Burlingame, CA, USA) for confocal microscopy analysis.

Luciferase assays

The transcriptional activity of the SERCA2 gene was evaluated using a firefly luciferase reporter gene as described previously (Vega *et al.* 2011). In brief, C2C12 cells were co-transfected with the purified recombinant chimeric hSERCA2/Luc plasmid, together with plasmids encoding EGFP, EGFP-PABPN1 or EGFP-PABPN1-17A (in a 1:2 molar ratio). The myotubes were then harvested in 1X passive lysis buffer (PBL; Promega), incubated 15 min (at RT with agitation) and frozen at −80°C.

Subsequently, the cell extracts were thawed (at RT), centrifuged (at 11,000 *g* for 2 min) and the supernatant was used to measure both firefly luciferase enzymatic activity and total protein (by the Bradford assay). Results are shown as arbitrary units, which represent luciferase bioluminescence normalized to the amount of total protein in the extract.

Quantitative real-time PCR assays

Total RNA was isolated from C2C12 myotubes using TRIzol Reagent (Invitrogen, Thermo Fisher Scientific Inc., Waltham, MA, USA), quantified on a NanoDrop ND-1000 spectrophotometer (Thermo Fisher Scientific Inc.) and reverse transcribed using a SuperScript First Strand Synthesis kit in accordance with the manufacturer's instructions. PCR was carried out in 20 μl, containing 10 μl of SYBR Green qPCR Ready Mix 2X, 1.5 μl of cDNA and 100 nM primer in a StepOnePlusTM Real-Time PCR System (Applied Biosystems, Foster City, CA, USA). Expression of CSQ2 was quantified by the $2\Delta\Delta$CT method, using GAPDH to normalize the data. Primer sequences were: GAPDH, forward 5′-GGAGAAACCTGCCAAGTATGATGAC-3′ and reverse 5′-TGGGAGTTGCTGTTGAAGTCG-3′ CSQ2, forward 5′-AGCTTGTGGAGTTTGTGAAG-3′ and reverse 5′-GGATTGTCAGTGTTGTCCC-3′.

Western blotting analysis

This procedure is based on a description reported previously (Vega *et al.* 2011). In brief, C2C12 myotubes were washed twice with PBS and then exposed to RIPA buffer consisting of (mM): 20 Tris-HCl (pH 7.5), 150 NaCl, 1 Na$_2$EDTA, 1 EGTA, 10 NaPyroPO$_4$, 10 β-glycerophosphate, 10 NaF and 1 Na$_3$VO$_4$; supplemented with 1% NP-40, 1% sodium deoxycholate and a proteinase inhibitor cocktail (Roche Diagnostics, Basel, Switzerland). Subsequently, protein samples (20–50 μg) were subjected to SDS-PAGE, transferred to polyvinylidene difluoride membranes and analysed by western blotting. The primary antibodies and dilutions used were: anti-RyR1 (ARR-001; Alomone Labs, Jerusalem, Israel; dilution 1:1000), anti-P-PBL (07-052; Upstate Biotechnology, Lake Placid, NY, USA; dilution 1:1500), anti-STIM1 (ACC-063; Alomone; dilution 1:1000) and anti-Orai1 (ACC-062; Alomone; dilution 1:500). Each particular membrane was also probed with an anti-β-tubulin antibody (32-2600; Invitrogen; dilution 1:4000) to normalize for the amount of protein loaded. Immunoreactivity was revealed by secondary antibodies coupled to peroxidase (either 32 260; Pierce Biotechnology, Rockford, IL, USA; dilution 1:15,000 or G-21040; Invitrogen; dilution 1:10,000). Band analysis was performed with ImageJ (NIH, Bethesda, MD, USA).

Fusion index

The fusion index was used as an indicator of the degree of terminal differentiation, as described previously (Vega *et al.* 2011). Briefly, C2C12 cells were co-transfected with a 3:1 molar ratio of cDNAs encoding green fluorescent proteins (either EGFP, EGFP-PABPN1 or EGFP-PABPN1-17A) and DsRed. Subsequently, the nuclei were stained with Hoechst, and fluorescence images were stored on the hard drive of a personal computer for off-line analysis. The images were taken using a digital camera (PowerShot, A720 IS; Canon, Tokyo, Japan), which was mounted onto an inverted microscope (IX71; Olympus, Tokyo, Japan) equipped with epifluorescence. The matching images were overlaid, and the fusion index was quantified as the percentage of nuclei contained in DsRed-positive myotubes with respect to the total nuclei per field.

Nuclear morphometry

Myotubes expressing EGFP, EGFP-PABPN1 or EGFP-PABPN1-17A were incubated with Hoechst. Subsequently, fluorescence images were collected with a confocal laser scanning microscope and the nuclear shape was analysed as reported previously (Rodríguez *et al.* 2015). Briefly, the nuclear contour ratio ($4\pi \times$ area $\times$ perimeter^{-2}) and the crossed diameter ratio (length $\times$ width^{-1}) were calculated using the measure function of the NIS-Elements software (Nikon).

Voltage clamp experiments

Intracellular Ca^{2+} transients and the activity of L-type Ca^{2+} channels were recorded simultaneously, as reported previously for C2C12 myotubes (Vega *et al.* 2011) and adult muscle fibres (Wang *et al.* 1999; Royer *et al.* 2008). Briefly, cells were placed into a recording chamber containing an external solution (see recording solutions). Subsequently, an internal solution was used to prepare patch electrodes, which exhibited electrical resistances of either 1–2 MΩ (fibres) or 2–3 MΩ (myotubes). Cell capacitance (C_m) was estimated from linear capacitive currents, which were acquired under both whole-cell and cell-attached conditions. The holding potential (HP) was set to -80 mV and brief membrane depolarizations to different potentials elicited Ca^{2+} currents and transients. For each cell, the peak value of Ca^{2+} current was normalized by C$_m$, and the respective current density was plotted as a function of V$_m$. The resulting *I*–*V* curves were fitted according to the function:

$$I = G_{max}(V_m - V_{rev})/\{1 + exp\,[(V_{G1/2} - V_m)/k_G]\} \quad (1)$$

where G_{max} represents the maximal conductance, V_{rev} is the apparent reversal potential, $V_{G1/2}$ is the potential at half-maximal activation of G_{max} and k_G is a slope factor.

Voltage-gated Ca^{2+} transients were measured using a Ca^{2+} fluorescent dye (either K_5 Fluo-4 or K_3 Rhod-2). A 100 W mercury arc lamp was used to excite the dye, in combination with filters and mirrors (in nm): 470–490 and 530–550 (excitation), 505 and 570 (dichroic), and 515–550 and 575–595 (emission) for Fluo-4 and Rhod-2, respectively. The fluorescence was measured from a small rectangular area, using a photomultiplier tube. When Fluo-4 was used, special care was taken to avoid (from the fluorescence recording area) the GFP-tagged proteins, which were restrained to the nucleus. In addition, significant differences in the magnitude of voltage-gated Ca^{2+} release, and which were originally found with Fluo-4, were also corroborated using Rhod-2. The magnitude of Ca^{2+} transients ($\Delta F/F$) was estimated as the peak fluorescence during test pulses (F) divided by that recorded at rest (F_b) − 1 (García & Beam, 1994). $\Delta F/F$ was plotted as a function of V_m and fitted according to the Boltzmann equation:

$$\Delta F/F = (\Delta F/F)_{max}/\{[1 + exp(V_{F1/2} - V_m)/k_F]\} \quad (2)$$

where $(\Delta F/F)_{max}$ represents the maximal amplitude of $\Delta F/F$, $V_{F1/2}$ is the potential required to obtain 50% of $(\Delta F/F)_{max}$ and k_F is a slope factor.

The activity of the DHPR was also obtained from analysing immobilization-resistant charge movement. This term refers to gating current that persists following a prepulse protocol used to immobilize charge movement as a result of fast inactivating sodium channels (Adams *et al.* 1990). In brief, the immobilization-resistant charge movement was estimated from the integral of non-linear capacitive currents, recorded at the onset (Q_{ON}) of brief (10 ms) depolarizations. The resulting Q_{ON} values were normalized by C_m, plotted as a function of V_m, and fitted according to the equation:

$$Q_{ON} = Q_{max}/\{1 + exp[(V_{Q1/2} - V_m)/k_Q]\} \quad (3)$$

where Q_{max} represents the maximal value of charge movement, $V_{Q1/2}$ is the voltage required to activate 50% of Q_{max} and k_Q is the steepness coefficient.

I_{SkCRAC} was also investigated, in C2C12 myotubes subjected to the whole-cell patch clamp technique. These experiments were performed as described by Yarotskyy & Dirksen (2012), with some modifications. After obtaining the whole-cell configuration, the HP was set at −80 mV and repetitive depolarizations were applied (at 0.5 Hz) with the aim of depleting the SR of Ca^{2+}; this point was reinforced by including a high concentration of EGTA (20 mM) into the internal recording solution. The stimulation protocol consisted of a 1 s depolarization (to 0 mV), followed by a brief 40 ms pulse to +40 mV (to keep

track of leakage currents). I_{SkCRAC} was estimated 80 ms after repolarization to the HP, according to:

$$I_{SkCRAC} = I_{-80} - I_{+40}(A/B) \quad (4)$$

where L_{-80} and I_{+40} are currents measured all through the stimulation protocol (at −80 mV and +40 mV), and A and B also represent currents obtained at −80 mV (A) and +40 mV (B) but before applying the first 1 s depolarizing step.

ECCE and basal levels of intracellular Ca^{2+}

Both basal levels of intracellular Ca^{2+} and excitation-coupled Ca^{2+} entry (ECCE) were investigated in intact, Indo-1 AM loaded myotubes, as described previously (Cherednichenko *et al.* 2004; Vega *et al.* 2011; Romberg *et al.* 2014). Briefly, cells were exposed 30 min to 6 μM of Indo 1 AM (in rodent Ringer), rinsed and incubated with DMEM (60 min at 37°C). When indicated, this incubation was performed with DMEM to which ryanodine (200 μM) was added. The dye was excited with a 100 W mercury arc lamp (at 335–345 nm) and fluorescence emissions were collected with two photomultiplier tubes (at 405 ± 15 nm, F_{405}; and 485 ± 12.5 nm, F_{485}). The levels of Ca^{2+} are expressed as fluorescence ratio ($R_{405/485}$), and the magnitude of ECCE is presented as the Δ Ratio. More precisely, the Δ Ratio stands for the maximal fluorescence ratio (triggered by high external K^+) minus its respective basal.

Recording solutions

Ca^{2+} currents and transients in C2C12 myotubes were recorded with the following solutions (in mM). *External*: 150 TEA-Cl, 10 $CaCl_2$ and 10 Hepes. *Internal*: 145 Cs-aspartate, 10 CsCl, 0.1 Cs_2-EGTA, 5 Mg-ATP, 10 Hepes and 0.2 of either K_5 Fluo-4 or K_3 Rhod-2. On the other hand, in adult muscle fibres, these measurements were performed with the following solutions (in mM). *External*: 140 TEA-CH_3SO_3, 10 Hepes, 1 $CaCl_2$, 2 $MgSO_4$, 5 4-aminopiridine, 1 9-anthracene carboxylic acid, 10 glucose, 0.025 *N*-benzyl-*p*-toluene sulphonamide and 0.001 TTX. *Internal*: 140 Cs-aspartate, 5 CsCl, 10 Cs-EGTA, 1 $CaCl_2$, 5 ATP-Mg, 10 Hepes and 0.1 K_3 Rhod-2.

The intramembrane charge movement was investigated in the presence of the same solutions as those for Ca^{2+} currents and transients (see above), except that they were supplemented with 0.5 mM $CdCl_2$, 0.003 mM TTX and either 0.1 mM or 0.3 mM $LaCl_3$ (for myotubes and muscle fibres, respectively). In addition, the *Internal* solution for myotubes consisted of (mM): 134 Cs-aspartate, 10 Cs_2-EGTA, 5 $MgCl_2$ and 10 Hepes.

Recording solutions for I_{SkCRAC} were (in mM): 138 TEA-CH_3SO_3, 10 $CaCl_2$, 1 $MgCl_2$, 10 Hepes and

0.1 nifedipine (*External*) and 140 Cs-CH$_3$SO$_3$, 20 Cs-EGTA, 4 MgCl$_2$ and 10 Hepes (*Internal*).

Basal levels of Ca^{2+} were assessed in the presence of rodent Ringer, consisting of (mM): 145 NaCl, 5 KCl, 2 CaCl$_2$, 1 MgCl$_2$ and 10 Hepes. ECCE was evoked with 80 mM K$^+$, which was incorporated into rodent Ringer by substituting for 75 mM Na$^+$. In these experiments, caffeine (30 mM, dissolved in Ringer) was applied immediately before K$^+$ to determine whether a preincubation with ryanodine effectively eliminated SR Ca^{2+} release.

In all solutions, the pH was adjusted to 7.3, and the experiments were performed at RT ($\sim$24°C). Both caffeine and K$^+$ were applied locally, using a fast perfusion system (SF-77B; Warner Instruments, Hamden, CT, USA).

Statistical analysis

Data were analysed with SigmaPlot (Systat Software Inc., San Jose, CA, USA) and pCLAMP (Molecular Devices, Sunnyvale, CA, USA). Data are expressed as the mean $\pm$ SEM of the indicated number of experiments (*n*). Statistical analysis was performed with Student's *t* tests (two-tailed). $P < 0.05$ (corrected for multiple comparisons) was considered statistically significant.

Results

Both PABPN1 and PABPN1-17A shape the morphology of C2C12 myotubes

It is well known that PABPN1 stimulates the fusion or terminal differentiation of myoblasts (Kim *et al.* 2001; Apponi *et al.* 2010; Anvar *et al.* 2013). Thus, we first explored whether the PABPN1-17A mutant protein can reproduce this function. Accordingly, cells were co-transfected with cDNAs encoding DsRed and either EGFP (Control), PABPN1 or PABPN1-17A. The nucleus was also stained with Hoechst, which allowed us not only to confirm the nuclear distribution of the two PABPN1 proteins (Fig. 1*A*, columns 2 and 3), but also to quantify myotube formation (analysing the fusion of myoblasts). As can be seen in Fig. 1*B*, the fusion index was increased by two-fold in response to PABPN1. However, PABPN1-17A failed to mimic this effect (Fig. 1*B*). These data support the notion that PABPN1 exerts a critical role in myogenesis. Moreover, they also suggest that the OPMD pathology could originate from a disrupted ability of PABPN1 mutant proteins to stimulate myotube formation.

In Fig. 1*A*, it can be seen that PABPN1 and PABPN1-17A exhibit a clear nuclear distribution. This characteristic, coupled with the fact that OPMD involves the presence of INIs, prompted us to examine the morphology of this organelle. This was accomplished by transfecting myotubes with either EGFP (Control) or DsRed

plus PABPN1 or PABPN1-17A. In addition, the nuclei were stained with Hoechst. At the confocal microscope (Fig. 2*A*), the nuclei of PABPN1-17A-expressing myotubes appeared smaller, more ovoid and their contour was highly irregular (Fig. 2*A*, lower right) compared to the other experimental conditions (Fig. 2*A*). Also, PABPN1-17A promoted both a lower nuclear contour ratio (Fig. 2*B*) and an increased crossed diameter ratio (Fig. 2*C*), which account quantitatively for the morphological alterations; the former indicates a higher convoluted shape and the latter a more ovoid shape. These deformities probably result in an altered expression of numerous genes (Woringer *et al.* 2014), such as those 202 that were recently identified in response to PABPN1-13A, a PABPN1 mutant protein with three additional alanines (Corbeil-Girard *et al.* 2005). Evidently, the corresponding functional impact has yet to be clarified.

PABPN1-17A inhibits VGCR

Subsequently, we used myotubes of comparable size to avoid conflictive interpretations, related to degrees of maturation. In Fig. 3, for example, the average value for C_m (which is proportional to the amount of cell membrane) was similar for all experimental conditions. Specifically, C_m was (in pF): 78 ± 21, 96 ± 21 and 92 ± 13; for control, PABPN1- and PABPN1-17A-expressing myotubes. The ECC is critical to force development (Melzer *et al.* 1995) and hence we hypothesized that it might be altered by PABPN1-17A. This point was investigated using the whole-cell patch clamp technique in conjunction with the Ca^{2+} sensitive dye Fluo-4, which allowed us to monitor simultaneously VGCR (RyR1 function) and L-type Ca^{2+} channel activity (DHPR function). Figure 3 illustrates examples of the corresponding traces obtained for Ca^{2+} transients (Fig. 3*A*) and currents (Fig. 3*C*). PABPN1-17A-expressing myotubes exhibited transients of reduced amplitude (Fig. 3*A*, column 3) with respect to both control and PABPN1-expressing myotubes (Fig. 3*A*). By contrast, the current density did not significantly differ between the three experimental conditions (Fig. 3*C*). To provide a more quantitative estimation of these observations, the voltage-dependence of both Ca^{2+} currents (Fig. 3*D*) and transients (Fig. 3*B*) was fitted according to Eqns (1) and (2), respectively. All parameters describing these processes were similar among experimental conditions, except for the maximum transient amplitude ($\Delta F/F_{max}$) of PABPN1-17A-expressing cells, which was reduced to $\sim$60% (Fig. 3*B* and *D*; Table 1). Thus, PABPN1-17A strongly inhibits VGCR, in a manner that does not require alteration of either the density of L-type Ca^{2+} current or the respective voltage-dependence. This conclusion was further strengthened by obtaining an estimation of the SR Ca^{2+} release flux. Briefly, we calculated the peak value of the first derivative of the Ca^{2+}

transient, which represents a reasonable approximation of the maximal voltage-gated SR Ca^{2+} release flux ($\delta F/\delta t_{max}$, as reported previously) (Avila and Dirksen, 2005). More specifically, the average values of $\delta F/\delta t_{max}$ for Control-, PABPN1- and PABPN1-17A-expressing myotubes were (in $\Delta F/F\,s^{-1}$): 283 ± 52, 255 ± 41 and 163 ± 46 ($P < 0.05$ compared to both Control and PABPN1). Hence, these data support the interpretation that the OPMD mutation markedly inhibits the rate of Ca^{2+} release.

The results shown in Fig. 3 suggest that PABPN1-17A inhibits ECC without altering the activity of L-channels. However, because it is well known that the voltage-sensor of these channels triggers the opening of RyR1s (Rios & Brum, 1987; Tanabe *et al.* 1988), we investigated potential effects on the immobilization-resistant charge movement, which reflects the activity of the sensor (Fig. 4). Specifically, the integral of gating currents at the onset of depolarization (Q_{ON}) was calculated from current traces such as those shown in Fig. 4A. The resulting Q_{ON} values were plotted as a function of V_m, both in absolute terms (Fig. 4B) and normalized to its maximal value (Fig. 4C). Neither the voltage-dependence, nor the maximum value of Q_{ON} was altered in response to the expression of exogenous PABPN1s. These results indicate that the OPMD mutant inhibits ECC without affecting the function and expression of L-channels.
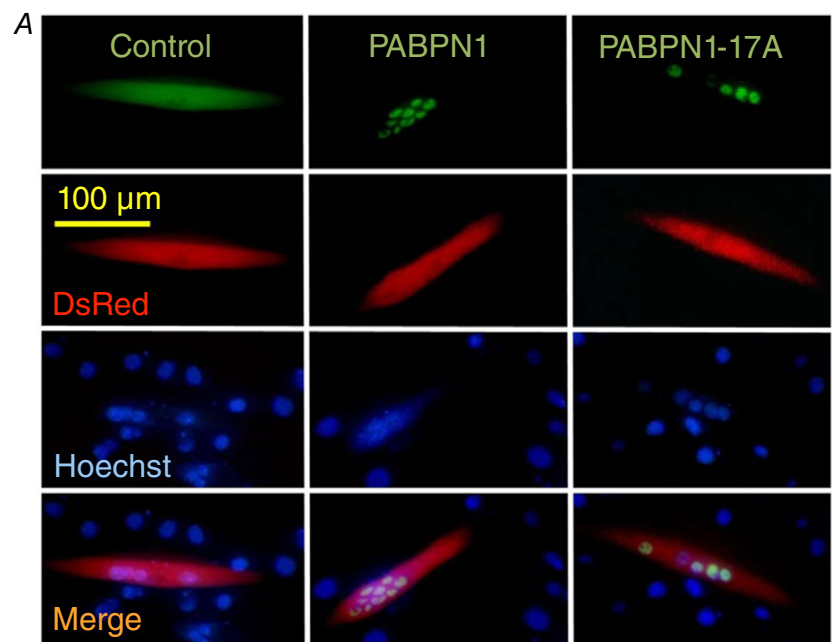

Figure 1. Expression of PABPN1, but not PABPN1-17A, stimulates the fusion of myoblasts

A, epifluorescence images of myotubes transfected with EGFP plus DsRed (Control), PABPN1 plus DsRed (PABPN1) and PABPN1-17A plus DsRed (PABPN1-17A). The myotubes were also labelled with Hoechst, to identify the nuclei. Note that both PABPN1 constructs exhibited a nuclear distribution (upper images). B, average values of fusion index that were estimated from images as those shown in (A). The numbers indicate the number of fields analysed. [Colour figure can be viewed at wileyonlinelibrary.com]

PABPN1-17A depletes the caffeine-sensitive SR Ca²⁺ store

We next surmised that the inhibition of ECC by the OPMD mutation might arise from a decreased SR Ca²⁺ load. If that were the case, then the caffeine-sensitive Ca²⁺ store should be depleted. This point was investigated under whole-cell patch clamp conditions (Fig. 5), using Rhod-2 as Ca²⁺ sensitive dye (instead of Fluo-4) (Fig. 3). The protocol consisted of applying a brief membrane depolarization (Fig. 5*A*, upper traces), followed by a fast delivery of 30 mM caffeine (Fig. 5*A*, lower traces). As predicted, from the results obtained with Fluo-4 (Fig. 3), in this experimental series, the expression of PABPN1-17A also resulted in a lower magnitude of Ca²⁺ transients elicited by voltage, confirming that this mutant protein inhibits VGCR. This finding is illustrated in both representative traces of Ca²⁺ transients (Fig. 5*A*, upper traces) and average values of the respective peak magnitude (Fig. 5*B*, voltage response). Notably, the PABPN1 mutant protein also reduced the magnitude of Ca²⁺ transients induced by caffeine (Fig. 5*A*, lower traces, and Fig. 5*C*). The degree of reduction was comparable for both responses (to caffeine and voltage). Indeed, the voltage-to-caffeine response ratio was unaltered (Fig. 5*D*), indicating that the inhibition of ECC is at least partially a result of decreased SR Ca²⁺ content.

The depletion of SR Ca²⁺ elicited by PABPN1-17A (Fig. 5, caffeine response) probably arises from a possible imbalance between SR Ca²⁺ leak and uptake.

Thus, we looked for evidence in support of such mechanism. However, neither the half-width of Ca²⁺ transient (Fig. 5*E*), nor the corresponding time constant of decay (Fig. 5*F*) was statistically different between control, PABPN1 and PABPN1-17A myotubes, suggesting that the PABPN1 constructs do not alter the overall SERCA activity. Similarly, the levels of $\Delta F/F$ that were observed after 10 s of electrical stimuli, and which might indicate the degree of SR Ca²⁺ leak, were similar across all experimental conditions (Fig. 5*G*). Thus, it is possible that PABPN1-17A promotes SR Ca²⁺ depletion through a cardiac-like 'invisible' leak (Bers, 2014), which in turn might be associated to altered steady-state Ca²⁺ fluxes.

Effects on resting intracellular Ca²⁺ and slow Ca²⁺ entry mechanisms

We next aimed to investigate two slow mechanisms of Ca²⁺ entry that coexist in skeletal muscle, termed: ECCE and store-operated calcium entry (SOCE). The latter is a result of the influx of Ca²⁺ via Orai channels and is assumed to participate in replenishing the SR pool of Ca²⁺ (Dirksen, 2009). The respective Ca²⁺ release-activated Ca²⁺ channel current in primary skeletal myotubes (I_{SkCRAC}) was characterized recently as an inward Ca²⁺ current that activates after depleting the SR Ca²⁺ with repetitive stimulation and the presence of a high concentration of a Ca²⁺ chelator (Yarotskyy & Dirksen, 2012). Thus, we used the I_{SkCRAC} as an indicator of SOCE and compared
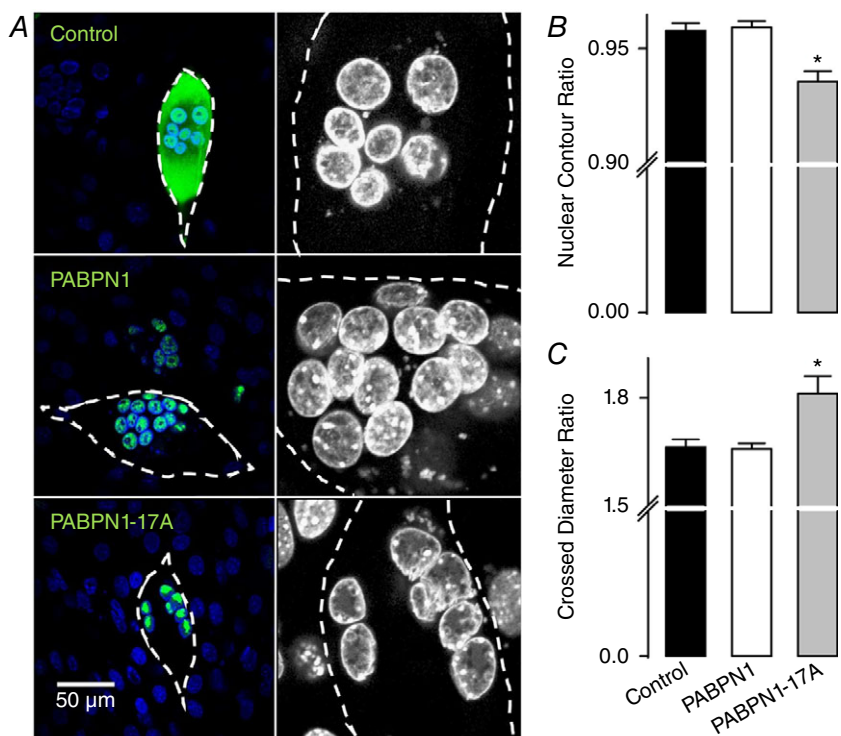

Figure 2. The PABPN1-17A OPMD mutation alters the nuclear structure
A, confocal images of fluorescence obtained from myotubes transfected as indicated in Fig. 1, except that DsRed was excluded in control myotubes. The calibration bar applies to the images on the left, which represent fluorescence corresponding to both EGFP and Hoechst. Dashed lines illustrate the contour of myotubes. The area nearby to nuclei was amplified in the images on the right, which show only the Hoechst signal (in grey scale) to emphasize the morphology of nuclei. *B* and *C*, average values of both nuclear contour (*B*) and crossed diameter (*C*), which are ratios that were estimated from images as in (*A*) ($n = 20$, for each experimental condition). [Colour figure can be viewed at wileyonlinelibrary.com]

it between control myotubes and those expressing either PABPN1 or PABPN1-17A (Fig. 6*A* and *B*).

Figure 6*A* shows raw current values that were obtained from naïve myotubes, using a stimulation protocol that was designed to elicit I_{SkCRAC} (see Methods). The current values grow steadily and then decrease in response to a brief application of two well-known inhibitors of SOCE (Fig. 6*A*). These data indicate that, similar to the observations in primary skeletal myotubes (Yarotskyy & Dirksen, 2012), the C2C12 myotubes also express I_{SkCRAC}. The magnitude of this current was then estimated as a function of time according to Eqn (4) (which assumes a zero value before the stimulation protocol, and also corrects for the leak measured at +40 mV). Interestingly, the results obtained were comparable among the three experimental groups, suggesting that neither PABPN1, nor PABPN1-17A significantly alters SOCE (Fig. 6*B*).

In the next experimental series, we investigated ECCE, and in parallel measured the resting levels of cytosolic Ca^{2+}. These experiments were performed in intact, Indo-1 AM-loaded myotubes. A preincubation with ryanodine was used to prevent a possible contamination of ECCE with SR Ca^{2+} release, and this point was confirmed by the lack of caffeine-induced Ca^{2+} release (Fig. 6*C*, caffeine). The cells were depolarized with 80 mM K^+, which elicited an increase in cytosolic Ca^{2+} that reflects ECCE (Fig. 6*C*, K^+). Interestingly, cells expressing either PABPN1 or PABPN1-17A exhibited a ~35% reduction in ECCE, compared with controls (Fig. 6*C* and *D*). On the other hand, although neither PABPN1, nor PABPN1-17A altered levels of cytosolic Ca^{2+} at rest (Fig. 6*E*), both constructs markedly reduced these levels following exposure to ryanodine (Fig. 6*C*–*F*), apparently because of the lower magnitude of ECCE. Thus, a normal function of PABPN1 is to inhibit the mechanism underlying ECCE, and the OPMD mutation does not interfere with this action. Moreover, because the influx of Ca^{2+} via L-channels is considered to underlie ECCE (Bannister *et al.* 2009;
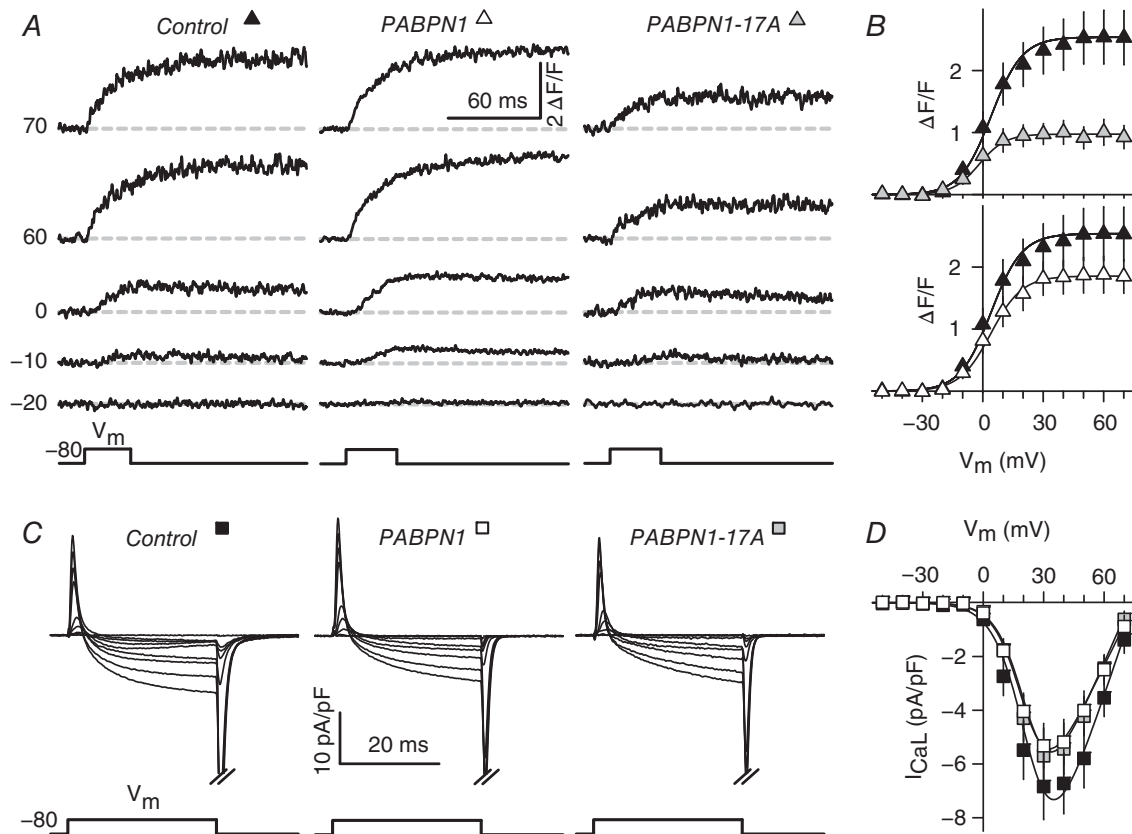

Figure 3. PABPN1-17A down-regulates ECC
A, examples of Ca^{2+} transients that were elicited by voltage and recorded from Ds-Red- (Control), PABPN1- and PABPN1-17A-expressing myotubes. The potential during test pulses is also illustrated (numbers on the left). *B*, averaged magnitude of Ca^{2+} transients plotted as a function of V_m, for both PABPN1-17A- (upper, grey symbols) and PABPN1-expressing myotubes (lower, open symbols). The respective data for control myotubes (closed symbols) are shown for clarity. *C* and *D*, representative L-type Ca^{2+} currents (*C*), recorded in myotubes, as shown in (*A*). The corresponding average current-to-voltage relationships are shown in (*D*). Both the number of experiments and parameters describing the voltage-dependence of Ca^{2+} transients ($\Delta F/F$-V data) and currents (*G*–*V* data) are presented in Table 1.

Table 1. Parameters of fitted *I–V*, *ΔF/F–V* and *Q–V* curves

			Control	PABPN1	PABPN1-17A
ΔF/F–V data	$(\Delta F/F)_{max}$		2.5 ± 0.4	1.9 ± 0.3	1.0 ± 0.2*
	k_F	mV	7.7 ± 0.7	7.7 ± 0.4	6.5 ± 0.9
	$V_{F1/2}$	mV	4.1 ± 2.5	4.0 ± 1.6	−1.9 ± 1.8
I–V data	G_{max}	nS nF^{-1}	223 ± 42	153 ± 18	171 ± 27
	k_G	mV	7.7 ± 0.5	6.9 ± 0.2	7.0 ± 0.3
	$V_{G1/2}$	mV	23.9 ± 2.1	21.6 ± 1.3	23.0 ± 1.6
	V_{rev}	mV	75.5 ± 2.4	75.4 ± 2.1	73.1 ± 3.1
	n		13	9	9
Q–V data	Q_{max}	nC μF^{-1}	3.1 ± 0.2	3.0 ± 0.3	2.9 ± 0.2
	K_Q	mV	19.8 ± 0.8	16.8 ± 1.0	19.5 ± 1.5
	$V_{Q1/2}$	mV	19.2 ± 2.5	13.3 ± 2.2	18.3 ± 2.5
	n		16	19	15

Parameters were obtained from the number of indicated myotubes (*n*) and by fitting data shown in Figs 3 and 4 to Eqn (1), *I–V*; Eqn (2), *ΔF/F–V*; and Eqn (3), *Q–V*. *ΔF/F–V* and *I–V* data are from the same cells. *Significant difference compared to both control and PABPN1-expressing myotubes.

Dirksen, 2009; Robin & Allard, 2015), these data also suggest that the expression of PABPN1 proteins interfere with the conformational state that keeps these channels open under long depolarization. Noteworthy, although none of the PABPN1 proteins significantly decreased the density of Ca^{2+} current during short depolarizations (30 ms), both of them generated a clear tendency of the currents to be smaller than controls (Fig. 3*C* and *D*; Table 1).

Expression levels of proteins involved in the homeostasis of Ca^{2+}

Because both PABPN1 and PABPN1-17A induce lower levels of cytosolic Ca^{2+} (Fig. 6*C–F*), we considered whether this effect has an impact on the expression of the SERCA2 gene, which is Ca^{2+}-dependent (Vega *et al.* 2011). This was addressed by measuring the luciferase activity in myotubes transfected with a SERCA2-promoter/Luc-gene construct (Vega *et al.* 2011). Interestingly, both PABPN1
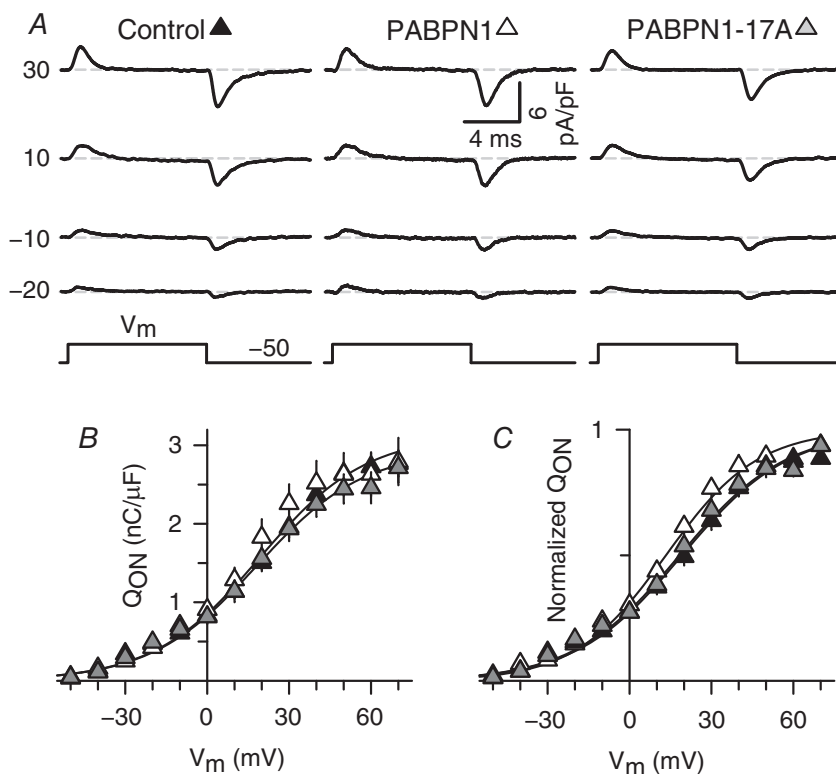

Figure 4. Neither PABPN1, nor PABPN1-17A alters the immobilization-resistant charge movement

A, examples of gating currents associated with the activity of L-channels, also known as immobilization-resistant charge movement. *B*, amount of charge that moves in response to depolarization (Q_{ON}) estimated as the time integral of outward gating currents recorded as in (*A*) for several membrane potentials (V_m). *C*, same data as in (*B*) but normalized by their respective maximal values (Q_{max}). Average values of Q_{max}, along with the corresponding half-activation voltage ($V_{Q1/2}$), slope factor (K_Q) and number of experiments are provided in Table 1 (*Q–V* data).

and PABPN1-17A gave rise to significant reductions in luciferase activity (Fig. 7A), indicating a decreased expression of the SERCA2 gene. The degree of inhibition, however, was different between PABPN1 and PABPN1-17A (80% and 50%, respectively). The expression levels of SERCA2 protein were next measured by immunofluorescence. Surprisingly, in contrast to the inhibition of gene expression (Fig. 7A), SERCA2 levels

were either unaltered (by PABPN1) or elevated (by PABPN1-17A, Fig. 7B). Because each of the experimental conditions exhibited different levels of SERCA2 gene expression (Fig. 7A), in Fig. 7C, we normalized immunofluorescence data (Fig. 7B) by their respective luciferase activity (Fig. 7A). This analysis revealed that, compared to controls (Fig. 7C), PABPN1 stimulated the relative expression efficiency of the SERCA2 gene by 6.4-fold
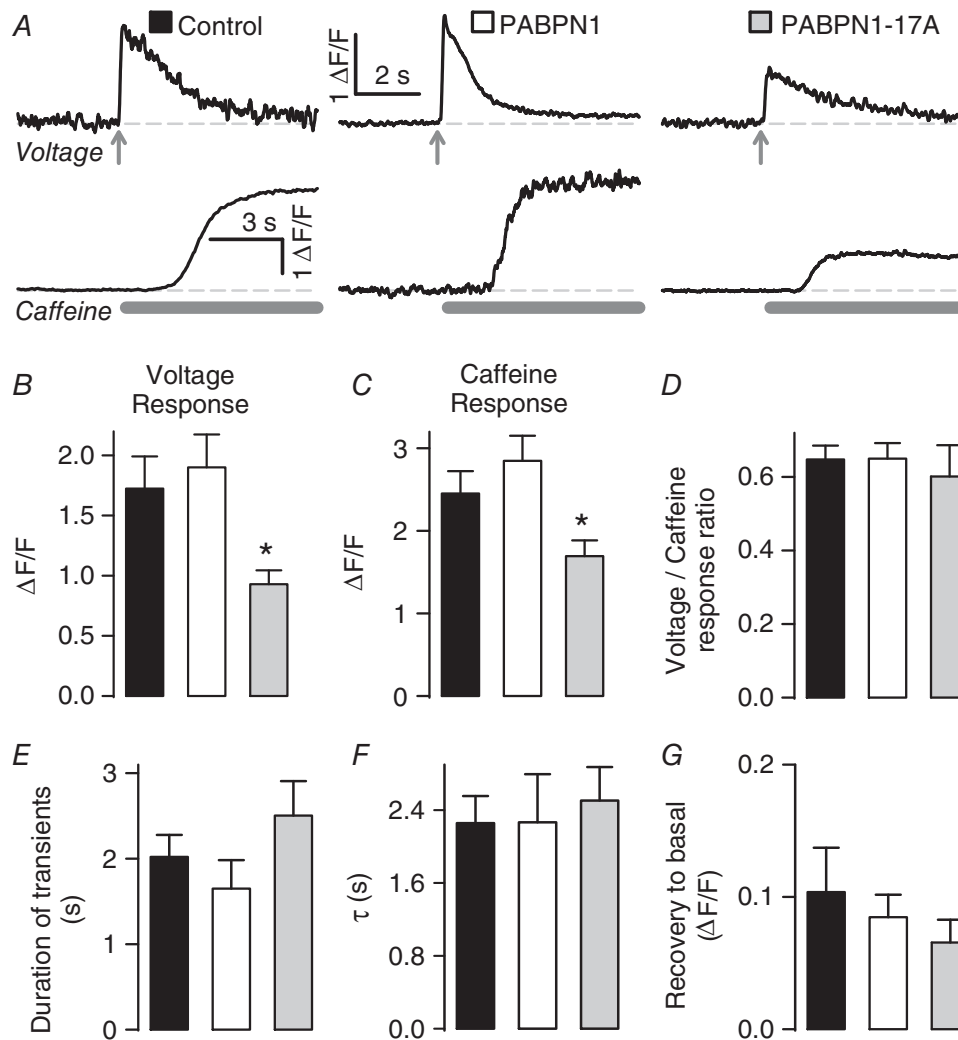

Figure 5. The OPMD mutation in PABPN1 inhibits voltage- and caffeine-evoked Ca^{2+} release without altering the kinetics of Ca^{2+} transient decay

A, examples of increases in $[Ca^{2+}]_i$ that were induced by either membrane depolarization (Voltage, upper traces) or caffeine exposure (Caffeine, lower traces). Recordings are from six individual myotubes expressing either EGFP (Control, left traces), PABPN1 (middle traces) or PABPN1-17A (right traces). For each experimental condition, a brief depolarizing pulse (of 30 ms, to +70 mV; arrows) was applied, followed by local delivery of caffeine (30 mM, in Ca^{2+}-free external solution added with 0.5 mM of EGTA). B and C, average increases in $[Ca^{2+}]_i$ that were elicited from experiments as in (A), in response to (B) voltage and (C) caffeine. D, voltage-to-caffeine response ratio, estimated as the magnitude of increases in $[Ca^{2+}]_i$ induced by voltage (B), divided by that corresponding to caffeine (C). E–G, termination kinetics of Ca^{2+} transients elicited as in (A) (Voltage). The decaying phase of the transient was analysed for: (E) time to half of the peak value, (F) time constant (obtained by fitting the data to a single exponential function) and (G) absolute value following 10 s of the stimulus. Data are from 36 Control (closed symbols), 27 PABPN1- (open symbols) and 30 PABPN1-17A-expressing (grey symbols) myotubes. The levels of Ca^{2+} were monitored with Rhod-2.

(Fig. 7*C*). However, the PABPN1 mutant protein only enhanced this parameter by 3.2-fold (Fig. 7*C*). These data suggest that PABPN1 and PABPN1-17A exert different posttranscriptional effects on the stability of SERCA2 mRNA and/or protein. In theory, the overexpression of SERCA2 protein induced by PABPN1-17A (Fig. 7*B*) may reflect a compensatory mechanism, which nevertheless failed to replenish a reduced pool of SR Ca^{2+} (Fig. 5).
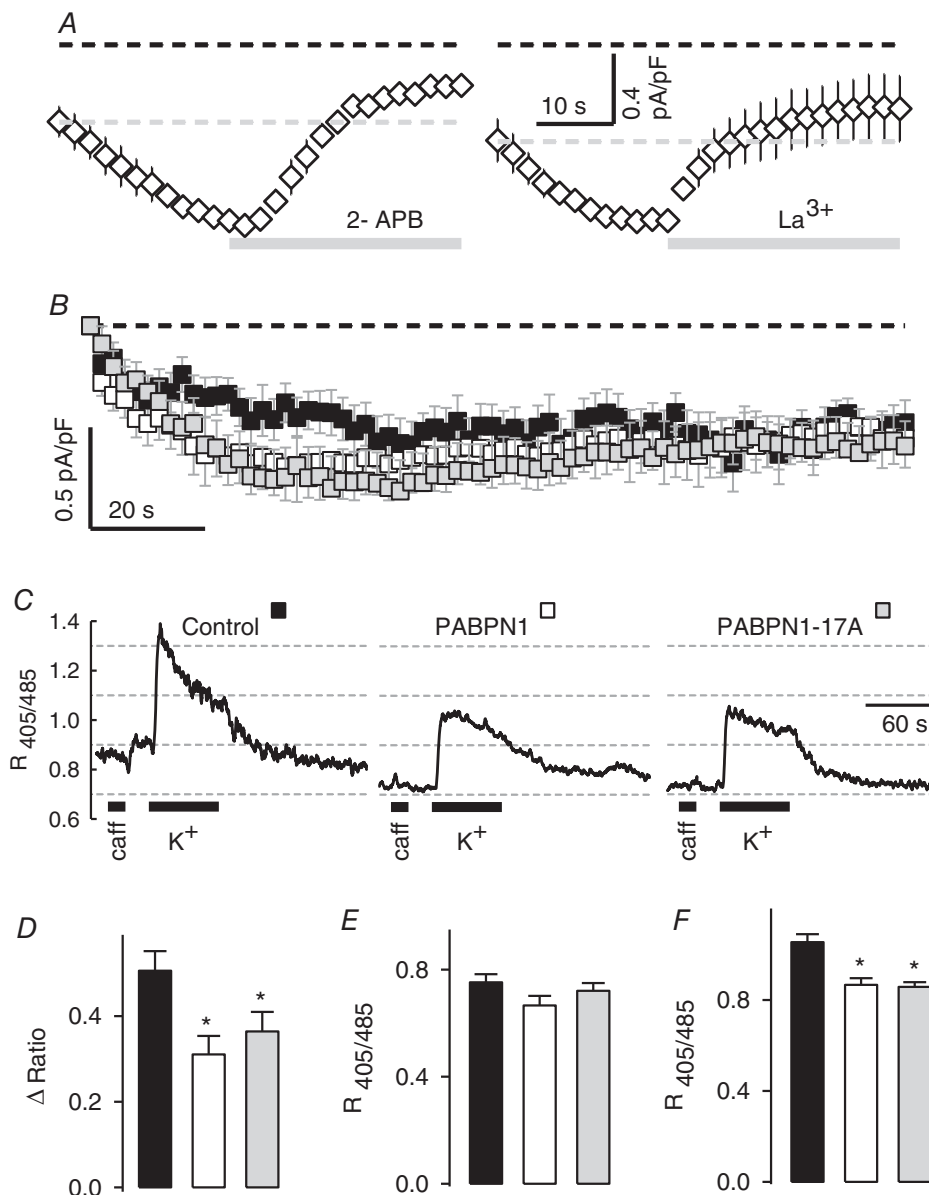

Figure 6. Effects on I_{SkCRAC}, ECCE and resting cytosolic Ca^{2+}
A, values of I_{Ca} density that were measured under recording conditions designed to study I_{SkCRAC} (under repetitive stimulation at 0.5 Hz). Dashed black lines illustrate the absolute zero value. The results were obtained from naïve C2C12 myotubes and are shown normalized to the magnitude of current measured before the addition of either 2-APB (75 μM, $n = 3$) or La^{3+} (10 μM, $n = 3$). In each plot, a dashed grey line illustrates I_h, the current value observed immediately before applying the stimulation protocol. The fact that both La^{3+} and 2-APB abate the protocol-induced current suggests the current reflects I_{SkCRAC}. *B*, average values of I_{SkCRAC} that were estimated as in (*A*) but corrected according to Eqn (4). Data are from 11 control (closed symbols), 23 PABPN1- (open symbols) and 15 PABPN1-17A-expressing (grey symbols) myotubes. *C*, traces of Indo-1 fluorescence ratio ($R_{405/485}$) reflecting the impact of ECCE on intracellular Ca^{2+}. SR Ca^{2+} release was eliminated by pre-incubating with ryanodine, which was corroborated by the absence of caffeine response (caff). ECCE was triggered by membrane depolarization with high external K^+ (K^+) and its average magnitude is shown in (*D*). The levels of cytosolic Ca^{2+} at rest are also presented, both before (*E*) and after ryanodine incubation (*F*, same cells as in *D*).

This view is further supported by the higher levels of SERCA2 protein not resulting in an acceleration of the decay phase of Ca^{2+} transients (compare Fig. 7*B* with Fig. 5*E–G*).

Calsequestrins are the main Ca^{2+} binding proteins inside the SR and thereby contribute to regulating the SR Ca^{2+} content (Royer & Ríos, 2009). To date, two different calsequestrin (CSQ) gene products have been identified in mammals: type 1 and type 2 (Yano & Zarain-Herzberg, 1994). Although C2C12 myotubes express the two iso-forms (Arai *et al.* 1991), knocking down CSQ2 but not CSQ1 leads to functional consequences, such as reduced SR Ca^{2+} content (Wang *et al.* 2006). This back-drop prompted us to investigate whether either PABPN1 or PABPN1-17A affects the steady-state levels of CSQ2 mRNA (Fig. 7*D*). However, although the levels of CSQ2 mRNA were indeed modified, they varied in a way that does not contribute to explaining differences in SR Ca^{2+} content. Specifically, they were increased by both PABPN1 and PABPN1-17A (Fig. 7*D*); thus, the reduced levels of SR Ca^{2+} induced by PABPN1-17A do not appear to arise from a potential down-regulation of CSQ2.

Next, we investigated whether the PABPN1-17A mutation influences the expression of phospholamban (PLB; which modulates SERCA activity), RyR1, STIM1 and Orai1. The phosphorylation of PLB at serine16 (phospho-PLB-Ser16 or P-PLB) removes tonic inhibition of SERCA (Vega *et al.* 2011). Thus, a potential reduction in the levels of P-PLB could explain the tendency of the Ca^{2+} transient to last longer in response to PABPN1-17A (Fig. 5*E*). Nevertheless, these levels were not significantly altered by any of the PABPN1 constructs (Fig. 8, *P-PLB*).

Similarly, these constructs did not alter the expression of STIM1 or Orai1 (Fig. 8), which is in keeping with the absence of effects on I_{SkCRAC} (Fig. 6*B*). With regard to the expression of RyR1, we found that the OPMD mutation produced a striking ~50% reduction (Fig. 8, *RyR1*). Both this finding and the store depletion showed in Fig. 5 (caffeine) could be sufficient to explain the reduced magnitude of VGCR.

The OPMD mutation does not alter ECC in adult muscle fibres

PABPN1 is expressed ubiquitously; thus, it is still not known why its mutant proteins primordially compromise the function of skeletal muscle, as well as why the symptoms of OPMD begin after midlife (Messaed & Rouleau, 2009; Banerjee *et al.* 2013). A possible explanation is that, in adults, the expression levels of PABPN1 markedly decrease, specifically in muscle fibres. Such specificity, combined with the absence of a normal allele in OPMD patients, may result in accelerated muscle degeneration, at least partially via myogenic defects (Anvar *et al.* 2013). Our findings show that PABPN1-17A is unable to mimic the stimulation of myotube formation by PABPN1 and also inhibits ECC in developing myo-tubes, which is entirely in keeping with this hypothesis. On the other hand, it is possible that PABPN1-17A also alters ECC in adult muscle fibres. To investigate this possibility, we measured both the activity of L-channels and its ability to induce SR Ca^{2+} release, in mature fibres transfected with PABPN1 and PABPN1-17A. More precisely, the FDB of adult mouse (6–8 weeks old) was transfected *in vivo*, as reported previously (DiFranco *et al.* 2009). The respective
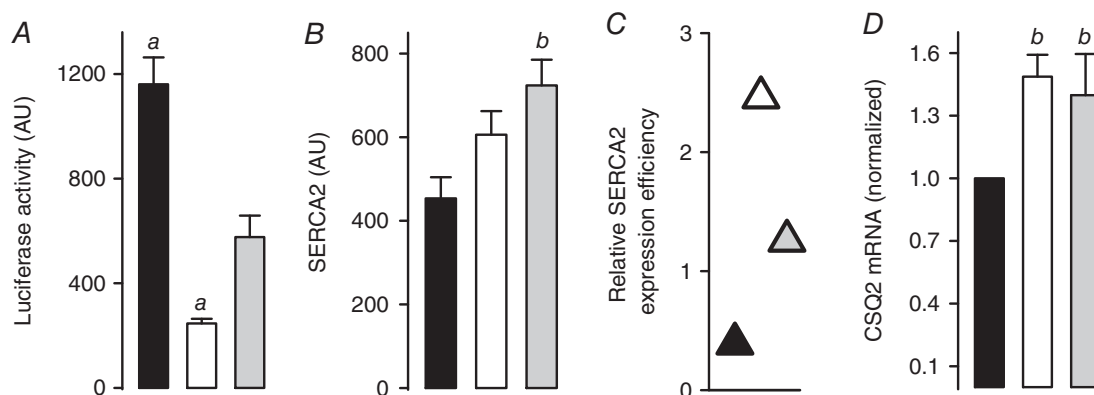

Figure 7. Expression levels of SERCA and calsequestrin
A and *B*, average expression levels of both SERCA2 gene (*A*) and protein (*B*). The former was assessed by luciferase activity and the latter by immunocytochemistry. *C*, relative SERCA2 expression efficiency, determined as the mean protein values (*B*) divided by those corresponding to gene transcription (*A*). *D*, levels of CSQ2 mRNA that were estimated by quantitative RT-PCR, using the ΔΔCt method. Data in (*A*) and (*D*) are from five and four independent determinations, respectively, for each experimental condition. Significant differences are also indicated compared to either PABPN1-17A (*a*) or Control (*b*). Closed, open and grey symbols denote, respectively: Control, PABPN1- and PABPN1-17A-expressing myotubes.

fibres were then isolated and subjected to whole-cell patch clamp to record simultaneously Ca^{2+} transients and either Ca^{2+} current or charge movement (Wang *et al.* 1999; Royer *et al.* 2008). Initially, the fibres were isolated 1 week after transfection and the corresponding results are presented in Fig. 9. Similar to the observations with C2C12 myotubes (Figs 1 and 2), the GFP fluorescence signal in adult muscle fibres also revealed a nuclear location of PABPN1 constructs (Fig. 9*A*). Remarkably, fibres expressing either PABPN1 or PABPN1-17A were indistinguishable with respect to not only the maximal values of Ca^{2+} transients [$(\Delta F/F)_{max}$] and Q_{ON} (Q_{max}), but also the corresponding voltage-dependence (Fig. 9*B–E* and Table 2). It is also noteworthy that the fibres transfected with PABPN1 and PABPN1-17A exhibited values of Ca^{2+} currents and transients that were comparable to those observed in controls (i.e. fibres transfected with EGFP only). For example, 1 week after transfection, the values of G_{max} (S F^{-1}) and $(\Delta F/F)_{max}$ obtained for EGFP- ($n = 8$),

PABPN1- ($n = 8$) and PABPN1-17A-expressing ($n = 11$) fibres, were, respectively: 126 ± 9.6, 167 ± 26 and 139 ± 13 for G_{max} and 7.0 ± 1.3, 5.9 ± 1.2 and 5.9 ± 1.2 for $(\Delta F/F)_{max}$. All these findings suggest that, in OPMD patients, muscle weakness does not arise from alterations in ECC of mature fibres.

On the other hand, because 1 week of PABPN1-17A expression may not recapitulate the alterations of the disease, we investigated fibres after a much longer period of transfection. Although the percentage of fibres expressing exogenous PABPN1s naturally decreased with time, it was possible to identify fibres expressing these proteins for as long as 5 months (i.e. in ~7-month-old mice). However, 5 month transfected fibres, with either PABPN1 or PABPN1-17A, were still identical with respect to the activity of L-channels (ionic current) and Ca^{2+} transients (Fig. 10 and Table 3). These results demonstrate that the long-term expression of PABPN1-17A does not alter the ECC of mature fibres.
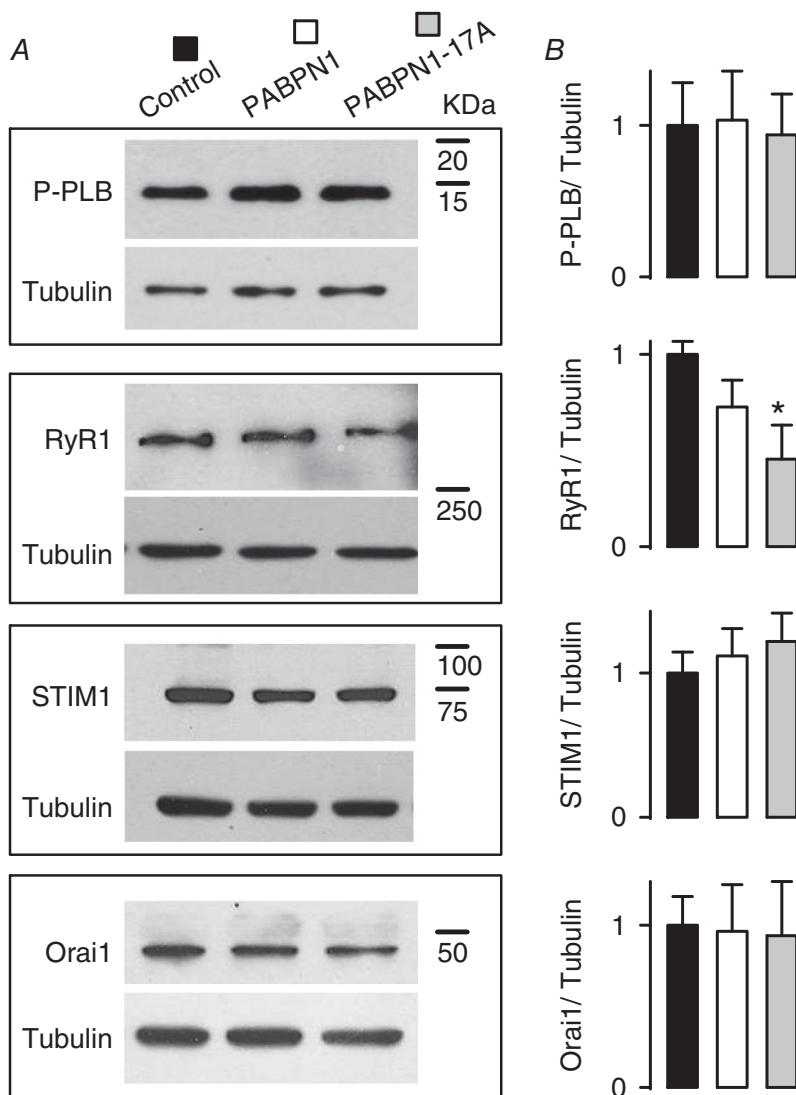

Figure 8. PABPN1-17A affects the expression of RyR1 but not of P-PLB, STIM1, or Orai1
A, examples of immunoblots investigated to assess the steady-state expression of P-PLB, RyR1, STIM1 and Orai1. β-tubulin was used to correct for variations in the amount of protein loaded. The brightness and contrast were adjusted to display similar backgrounds. *B*, band analysis for western blots as those shown in (*A*). The number of experiments is three in all cases. *P < 0.05 compared to Control.

Both the absence of PABPN1 and the ageing process result in decreased mitochondrial metabolic rate (Anvar *et al.* 2013). Thus, we investigated whether the mitochondrial uncoupler FCCP may be able to unravel alterations on ECC. Accordingly, Ca^{2+} transients were measured in 5 month transfected fibres, in the absence and presence of FCCP (Fig. 11). In accordance with a previous study, the application of FCCP resulted in a lower magnitude of Ca^{2+} transients (Caputo & Bolaños, 2008). However, the extent of this effect was the same regardless of the expression of PABPN1 or PABPN1-17A (Fig. 11 and Table 4). In skeletal muscle, the mRNA levels of PABPN1 decline with age (Anvar *et al.* 2013). Thus, we investigated whether PABPN1-17A alters ECC in fibres from aged mice. Specifically, we used animals at 1 year of age, instead of 6–8 weeks. However, after 1 week of

transfection, no changes were observed in the magnitude of either Ca^{2+} currents or transients when comparing the results obtained from fibres expressing each of the PABPN1 constructs (data not shown). Thus, PABPN1-17A disrupts ECC only in developing myotubes. Therefore, this effect could be relevant in the context of muscle remodelling.

Discussion

In skeletal muscle, Ca^{2+} is critical for a number of cellular processes, such as ECC, myoblast fusion and SERCA expression. If mutations in the PABPN1 gene give rise to altered expression and/or distribution of proteins that control the homeostasis of this ion, then such processes may also be altered, in a way that could contribute to explaining the pathophysiology of OPMD.
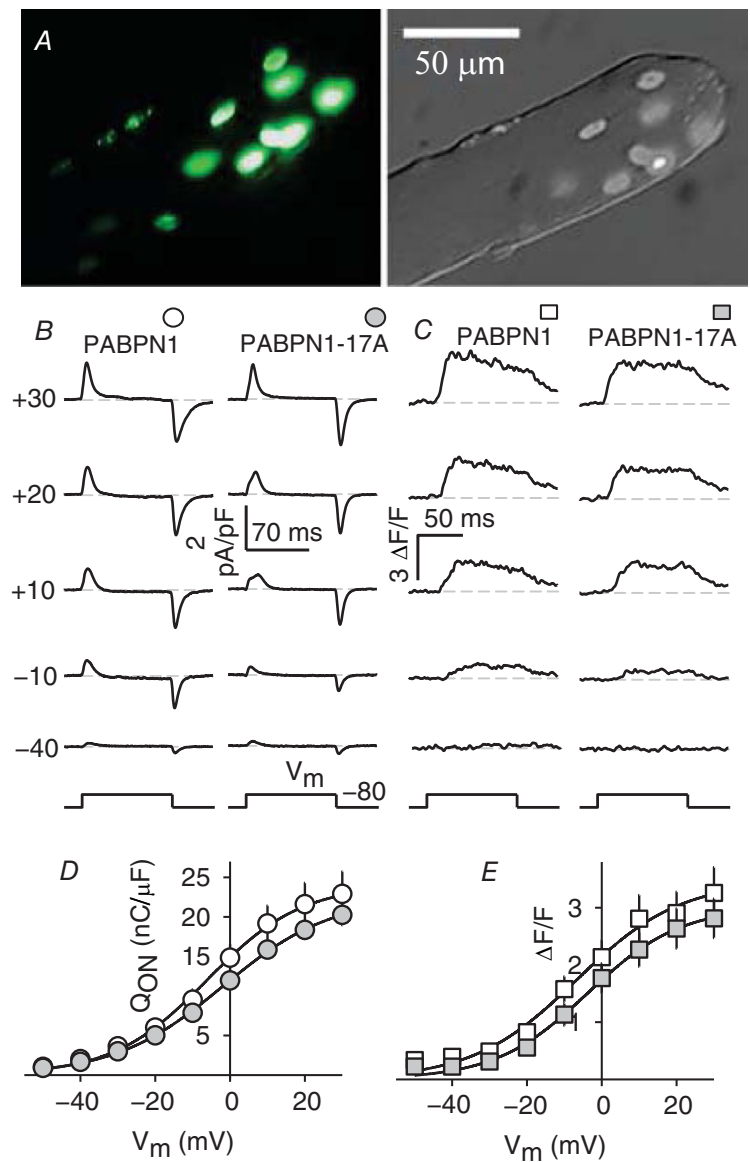

Figure 9. PABPN1-17A does not alter the ECC of adult muscle fibres in 1 week
A, representative images of epifluorescence (left) and brightfield (right) illustrating a muscle fibre obtained from a mouse of 7 weeks of age, which was transfected with 1 week of anticipation, using a plasmid containing the sequence for EGFP-PABPN-17A. Similar images were obtained for muscle fibres transfected with EGFP-PABPN1, both 1 week and 5 months after transfection. *B* and *C*, examples of charge movement (*B*) and Ca^{2+} transients (*C*) that were recorded in adult muscle fibres transfected (1 week) with either PABPN1 (open symbols) or PABPN1-17A (grey symbols). *D* and *E*, average voltage-dependence of charge movement (*D*) and Ca^{2+} transients (*E*) obtained as in (*B*) and (*C*), respectively. Data were fitted to Boltzmann equations, and the resulting parameters are provided in Table 2. [Colour figure can be viewed at wileyonlinelibrary.com]

Table 2. Parameters of fitted *Q–V* and *ΔF/F* curves, which were obtained from 1 week transfected muscle fibres

			PABPN1	PABPN1-17A
ΔF/F–V data	$(\Delta F/F)_{max}$		3.5 ± 0.5	2.9 ± 0.3
	k_F	mV	11.8 ± 1.3	9.1 ± 0.6
	$V_{F1/2}$	mV	-8.3 ± 2.5	-4.3 ± 2.3
Q–V data	Q_{max}	nC μF^{-1}	25.7 ± 3.3	22.70 ± 1.6
	k_Q	mV	13.1 ± 0.9	13.57 ± 0.6
	$V_{Q1/2}$	mV	-3.6 ± 1.6	-2.38 ± 1.7
	n		22	27

Parameters were obtained by fitting data shown in Fig. 9 to the appropriate equation: *ΔF/F–V*, Eqn (2) and *Q–V*, Eqn (3).

However, no study has systematically characterized the influence of PABPN1 mutant proteins in the homeostasis of Ca^{2+}. Consequently, we have evaluated the influence of PABPN1-17A on ECC, SOCE, ECCE, SR Ca^{2+} content, myoblast fusion, nuclear structure and expression levels of SERCA2, CSQ2, P-PLB, RyR1, STIM1 and Orai1. The results of the present study indicate that myotubes expressing PABPN1-17A exhibit a reduced magnitude of Ca^{2+} transients during ECC, and this effect was explained by lower levels of both SR Ca^{2+} content and

RyR1 expression. A decrease in ECCE could potentially contribute to explaining these effects, although it does not represent the main factor because it also occurred in PABPN1-expressing myotubes (which exhibit a normal level of both SR Ca^{2+} load and VGCR). Although SOCE represents another potential contributing factor, it does not appear to be involved because PABPN1-17A did not alter I_{SkCRAC}. On the other hand, because SOCE is considered to be important to limit fatigue in adult fibres (Wei-Lapierre *et al.* 2013), the possibility that PABPN1-17A alters not only these processes, but also the overall homeostasis of Ca^{2+} in these cells has yet to be fully investigated.

The OPMD symptoms may arise from alterations in myogenesis

Although genetic studies have clearly demonstrated linkage between mutations in PABPN1 and OPMD, the precise mechanism(s) by which these mutations give rise to the symptoms have yet to be firmly established. In particular, it remains unresolved why the symptoms only initiate at midlife, and also why the skeletal muscle is primarily affected. The latter point is particularly intriguing because PABPN1 is expressed ubiquitously
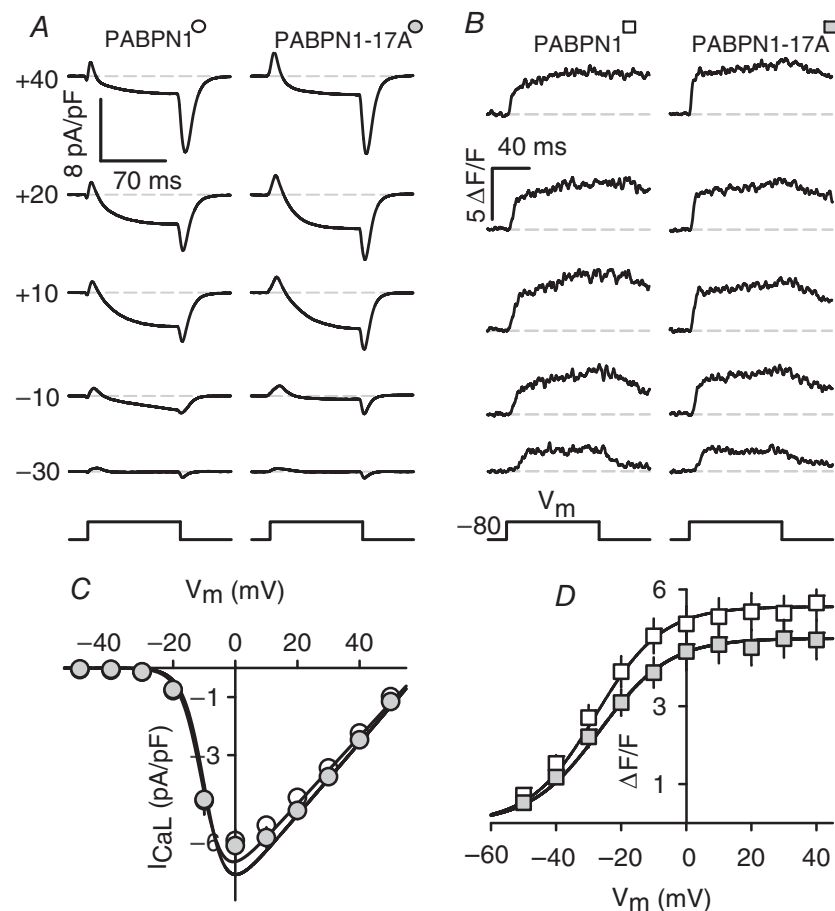

Figure 10. The PABPN1 mutant protein does not alter the ECC of adult muscle fibres in 5 months
A and *B*, representative traces of (*A*) L-type Ca^{2+} currents and (*B*) Ca^{2+} transients that were obtained from adult muscle fibres, 5 months after transfection (similar experimental conditions as in Fig. 9). The respective voltage-dependence and Boltzmann parameters are shown in (*C*) (currents), (*D*) (transients) and Table 3.

Table 3. Parameters of fitted *I–V* and *ΔF/F* curves, which were obtained from 5 month transfected fibres

			PABPN1	PABPN1-17A
ΔF/F–V data	$(\Delta F/F)_{max}$		5.6 ± 0.5	4.7 ± 0.5
	k_F	mV	10.1 ± 0.6	10.6 ± 0.7
	$V_{F1/2}$	mV	-27.8 ± 1.5	-26.6 ± 1.7
I–V data	G_{max}	nS nF^{-1}	116 ± 6.2	124 ± 7.5
	k_G	mV	3.4 ± 0.2	3.4 ± 0.3
	$V_{G1/2}$	mV	-10.4 ± 0.9	-9.4 ± 1.1
	V_{rev}	mV	60.3 ± 1.9	60.7 ± 2.1
	n		36	35

Parameters were obtained by fitting data shown in Fig. 10 to the appropriate equation: *I–V*, Eqn (1) and *ΔF/F–V*, Eqn (3).

(Abu-Baker & Rouleau 2006; Messaed & Rouleau, 2009; Banerjee *et al.* 2013). One possible explanation is that, although the levels of skeletal muscle PABPN1 normally decline with ageing, this process is accelerated in OPMD and thereby the functional impact of PABPN1 depletion should be exacerbated in OPMD (Anvar *et al.* 2013). Thus, our data provide support for the hypothesis that muscle atrophy and weakness in OPMD are both the result of an altered restoration of muscle mass arising from the inability of PABPN1 mutant proteins to stimulate myogenesis.

Molecular mechanisms underlying the effects of PABPN1 constructs

With regard to proteins that conform the couplon and thus directly or indirectly participate in ECC, the present study shows that PABPN1 constructs modify the expression of RyR1, SERCA2 and CSQ2. However, except for RyR1, the observed changes do not appear to have an impact on the homeostasis of Ca^{2+}. A possible explanation for this finding is that PABPN1 alters the expression of numerous proteins, whose functional impact might be compensatory. For example, a previous study showed that PABPN1 alters the expression and distribution of FKPB12, another protein of the couplon (Corbeil-Girard *et al.* 2005). That previous study also reported an extensive list of genes ($n = 202$) whose expression changes in response to either PABPN1 or PABPN1-13A (albeit that in an epithelial cell line, A549). Specifically, PABPN1-13A-expressing cells exhibited higher levels of FKPB12 mRNA than controls. Interestingly, however, the FKPB12 protein was trapped in the INIs of not only A549 cells, but also skeletal muscle biopsies from OPMD patients (Corbeil-Girard *et al.* 2005). In the couplon, FKBP12 binds to RyR1, and this interaction contributes to sustain normal levels SR Ca^{2+} release during ECC (Avila *et al.* 2003). Thus, lower levels of FKBP12 could potentially reinforce the

inhibition of ECC by PABPN1-17A. Interestingly, the PABPN1 constructs also alter the expression of S100P (a member of the S100 superfamily of EF-hand Ca^{2+}-binding proteins; Corbeil-Girard *et al.* 2005). Moreover, it has been reported that ECC is modulated by another member of this family (S100A) (Prosser *et al.* 2011). Thus, in the near future, it will be necessary to fully characterize the effects of OPMD mutations in all Ca^{2+}-handling proteins at the level of not only global expression, but also sub-cellular distribution. Accordingly, it is important to note that PABPN1-17A promotes a reduction in expression levels of troponin C (in C2C12 cells) (Wang & Bag, 2006). Thus, it is possible that alterations in proteins of the contractile machinery also form part of the etiology of OPMD. Accordingly, a recent study showed that not only is the splicing regulation of troponin T3 altered in skeletal muscle samples of OPMD patients, but also this alteration is linked to a right-shift in the force–Ca^{2+} relationship (Klein *et al.* 2016).

In our experiments, neither PABPN1, nor PABPN1-17A altered the kinetics of decay of Ca^{2+} transients elicited by
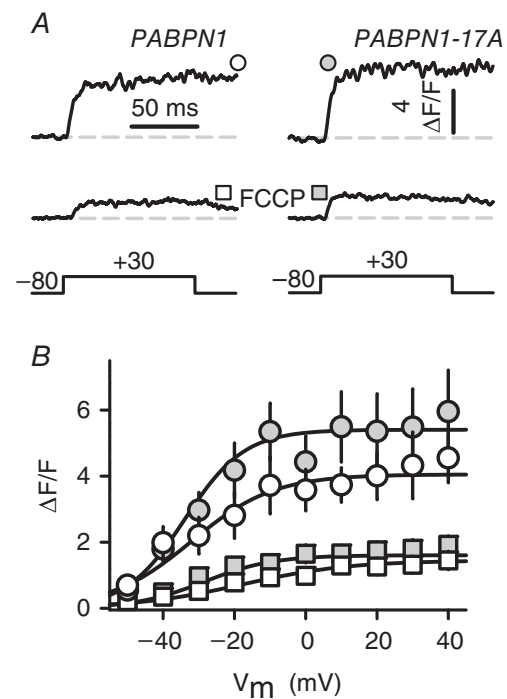
Figure 11. Effects of the mitochondrial uncoupler FCCP
A, examples of Ca^{2+} transients recorded in muscle fibres transfected (5 months) with either PABPN1 or PABPN1-17A, in the absence (upper traces) and presence (lower traces) of 2 μM FCCP. *B*, average voltage-dependence of Ca^{2+} transients recorded as in (*A*). The results are from 18 PABPN1- (open symbols) and 19 PABPN1-17A-expressing (grey symbols) fibres. The number of cells investigated in the absence (circles) and presence (squares) of FCCP is provided in Table 4, along with parameters describing voltage-dependence of not only Ca^{2+} transients, but also L-type Ca^{2+} currents.

Table 4. Parameters of fitted *I–V* and Δ*F/F–V* curves, which were obtained in the absence and presence of FCCP

	FCCP	n	*I–V* data				Δ*F/F–V* data		
			G_{max} (nS/nF)	k_G (mV)	$V_{G1/2}$ (mV)	V_{rev} (mV)	$(\Delta F/F)_{max}$	k_F (mV)	$V_{F1/2}$ (mV)
PABPN1	−	6	107 ± 18	4.9 ± 0.6	−9.3 ± 3.4	54.2 ± 6.2	4.0 ± 0.7	11.5 ± 1.5	−32.1 ± 4.9
	+	12	67 ± 12	6.2 ± 0.7	−10.4 ± 2.4	47.9 ± 4.9	1.4 ± 0.3	15.2 ± 1.4	−17.7 ± 4.4
PABPN1-17A	−	6	115 ± 13	3.1 ± 0.4	−11.1 ± 2.0	61.6 ± 3.9	5.4 ± 1.0	8.3 ± 1.0	−33.9 ± 3.6
	+	13	84 ± 9.3	5.0 ± 0.3	−11.5 ± 0.8	52.6 ± 2.6	1.7 ± 0.3	9.8 ± 1.4	−30.1 ± 2.1

Data are from the indicated number of 5 month transfected fibres (*n*). When indicated, FCCP (2 μM) was present in the external recording solution.

voltage. This suggests that there are no changes in the overall rates of SR Ca^{2+} leak and uptake, although it does not rule out possible alterations of both steady-state and microdomains. Thus, further work is needed to clarify the molecular basis of store depletion. The leak is hard to resolve. For example, in cardiac myocytes, it is often named 'invisible'. More precisely, this term stands for a 'dribble or seepage of Ca^{2+} out of the SR', which is not seen when monitoring Ca^{2+} with confocal microscopy (Bers, 2014).

The ECCE is considered to reflect an influx of Ca^{2+} via a fraction of L-channels that remain open during prolonged depolarizations (Bannister *et al.* 2009; Dirksen, 2009; Robin & Allard, 2015). Hence, it is noteworthy that the G_{max} of L-channels exhibited a tendency to be ~30% smaller in PABPN1- and PABPN1-17A-expressing myotubes compared to controls (Table 1). This observation, coupled with the fact that the magnitude of ECCE was significantly reduced in myotubes expressing each of the PABPN1 constructs, suggests that these proteins exert a minor inhibition of L-channel activity. The α2δ1 subunit of these channels represents a key component for sustaining ECCE (Gach *et al.* 2008). Thus, it will be interesting to investigate whether the two PABPN1s affect ECCE by down-regulating α2δ1 expression. Alternatively, the effect on ECCE could arise from a potential up-regulation of monomeric GTP-binding proteins (RGK), which were recently shown to impair this function of L-channels (Romberg *et al.* 2014).

A hallmark of laminopathies is present in OPMD

Abnormal cellular structures, similar to the INIs of OPMD, are commonly observed in neurodegenerative disorders termed the polyglutamine diseases, which are caused by trinucleotide repeat expansion of the CAG codon (Taylor *et al.* 2002; Abu-Baker & Rouleau, 2006). Such altered cell structures also occur in the myotonic dystrophy type 1 (DM1), which originates from an abnormal expansion of a CTG codon of the myotonic dystrophy protein kinase (DMPK) gene (Taneja *et al.* 1995). Similar to that observed with the OPMD mutation, DM1 mutations have also been

associated with an altered nuclear structure (Rodríguez *et al.* 2015). Thus, nuclear deformities, which are a hallmark of the laminopathies (Chi *et al.* 2009), apparently represent a trait shared by trinucleotide repeat disorders, and probably generate pleiotropy (Woringer *et al.* 2014). It is well known that the structure of the nucleus depends on proteins that shape the nuclear envelope, such as lamins and emerin (Chi *et al.* 2009). Accordingly, fibroblasts of DM1 patients that exhibit nuclear alterations also show an altered distribution of emerin and lamins A/C and B1 (Rodríguez *et al.* 2015). Thus, it is possible that nuclear deformities induced by PABPN1-17A are a result of potential alterations in the expression and/or distribution of these proteins, which clearly deserves further research. Similarly, a more comprehensive study has yet to be carried aiming to clarify the precise sequence of all of the effects of PABPN1-17A.

Conclusions

In conclusion, we have evaluated the functional impact of PABPN1 and PABPN1-17A in developing myotubes. The corresponding results indicate that the PABPN1-17A OPMD mutation both impairs ECC and is unable to stimulate myotube formation. These actions are the result of the reduced expression of RyR1, along with depletion of the intracellular Ca^{2+} store. PABPN1-17A also promotes alterations in nuclear structure and this effect probably generates pleiotropy. These findings greatly enlarge our knowledge about the effects of PABPN1 mutant proteins harbouring OPMD mutations. Moreover, they could also be part of the pathophysiology of this disease, in the context of skeletal muscle regeneration.

References

Abu-Baker A, Messaed C, Laganiere J, Gaspar C, Brais B & Rouleau GA (2003). Involvement of the ubiquitin-proteasome pathway and molecular chaperones in oculopharyngeal muscular dystrophy. *Hum Mol Genet* **12**, 2609–2623.

Abu-Baker A & Rouleau GA (2006). Chapter 33 - polyalanine and polyglutamine diseases: possible common mechanisms? A2 - Ashizawa, Robert D. WellsTetsuo. In *Genetic Instabilities and Neurological Diseases*, 2nd edn, pp. 487–513. Academic Press, Burlington. Available at: http://www.sciencedirect.com/science/article/pii/B978012369462150034X [Accessed 23 February 2016].

Adams BA, Tanabe T, Mikami A, Numa S & Beam KG (1990). Intramembrane charge movement restored in dysgenic skeletal muscle by injection of dihydropyridine receptor cDNAs. *Nature* **346**, 569–572.

Aihara H & Miyazaki J (1998). Gene transfer into muscle by electroporation in vivo. *Nat Biotechnol* **16**, 867–870.

Anderson JE, Wozniak AC & Mizunoya W (2012). Single muscle-fiber isolation and culture for cellular, molecular, pharmacological, and evolutionary studies. *Methods Mol Biol Clifton NJ* **798**, 85–102.

Anvar SY, Raz Y, Verway N, van der Sluijs B, Venema A, Goeman JJ, Vissing J, van der Maarel SM, 't Hoen PAC, van Engelen BGM & Raz V (2013). A decline in PABPN1 induces progressive muscle weakness in oculopharyngeal muscle dystrophy and in muscle aging. *Aging* **5**, 412–426.

Apponi LH, Corbett AH & Pavlath GK (2013). Control of mRNA stability contributes to low levels of nuclear poly(A) binding protein 1 (PABPN1) in skeletal muscle. *Skelet Muscle* **3**, 23.

Apponi LH, Leung SW, Williams KR, Valentini SR, Corbett AH & Pavlath GK (2010). Loss of nuclear poly(A)-binding protein 1 causes defects in myogenesis and mRNA biogenesis. *Hum Mol Genet* **19**, 1058–1065.

Arai M, Alpert NR & Periasamy M (1991). Cloning and characterization of the gene encoding rabbit cardiac calsequestrin. *Gene* **109**, 275–279.

Avila G & Dirksen RT (2005). Rapamycin and FK506 reduce skeletal muscle voltage sensor expression and function. *Cell Calcium* **38**, 35–44.

Avila G, Lee EH, Perez CF, Allen PD & Dirksen RT (2003). FKBP12 binding to RyR1 modulates excitation-contraction coupling in mouse skeletal myotubes. *J Biol Chem* **278**, 22600–22608.

Banerjee A, Apponi LH, Pavlath GK & Corbett AH (2013). PABPN1: molecular function and muscle disease. *FEBS J* **280**, 4230–4250.

Bannister RA, Pessah IN & Beam KG (2009). The skeletal L-type Ca(2+) current is a major contributor to excitation-coupled Ca(2+) entry. *J Gen Physiol* **133**, 79–91.

Beam KG & Franzini-Armstrong C (1997). Functional and structural approaches to the study of excitation-contraction coupling. *Methods Cell Biol* **52**, 283–306.

Benavides Damm T & Egli M (2014). Calcium's role in mechanotransduction during muscle development. *Cell Physiol Biochem Int J Exp Cell Physiol Biochem Pharmacol* **33**, 249–272.

Bers DM (2014). Cardiac sarcoplasmic reticulum calcium leak: basis and roles in cardiac dysfunction. *Annu Rev Physiol* **76**, 107–127.

Blumen SC, Brais B, Korczyn AD, Medinsky S, Chapman J, Asherov A, Nisipeanu P, Codère F, Bouchard JP, Fardeau M, Tomé FM & Rouleau GA (1999). Homozygotes for oculopharyngeal muscular dystrophy have a severe form of the disease. *Ann Neurol* **46**, 115–118.

Brais B, Bouchard JP, Xie YG, Rochefort DL, Chrétien N, Tomé FM, Lafrenière RG, Rommens JM, Uyama E, Nohira O, Blumen S, Korczyn AD, Heutink P, Mathieu J, Duranceau A, Codère F, Fardeau M, Rouleau GA & Korcyn AD (1998). Short GCG expansions in the PABP2 gene cause oculopharyngeal muscular dystrophy. *Nat Genet* **18**, 164–167.

Calado A, Tomé FM, Brais B, Rouleau GA, Kühn U, Wahle E & Carmo-Fonseca M (2000). Nuclear inclusions in oculopharyngeal muscular dystrophy consist of poly(A) binding protein 2 aggregates which sequester poly(A) RNA. *Hum Mol Genet* **9**, 2321–2328.

Caputo C & Bolaños P (2008). Effect of mitochondria poisoning by FCCP on Ca^{2+} signaling in mouse skeletal muscle fibers. *Pflüg Arch Eur J Physiol* **455**, 733–743.

Cherednichenko G, Hurne AM, Fessenden JD, Lee EH, Allen PD, Beam KG & Pessah IN (2004). Conformational activation of Ca^{2+} entry by depolarization of skeletal myotubes. *Proc Natl Acad Sci USA* **101**, 15793–15798.

Chi Y-H, Chen Z-J & Jeang K-T (2009). The nuclear envelopathies and human diseases. *J Biomed Sci* **16**, 96.

Corbeil-Girard L-P, Klein AF, Sasseville AM-J, Lavoie H, Dicaire M-J, Saint-Denis A, Pagé M, Duranceau A, Codère F, Bouchard J-P, Karpati G, Rouleau GA, Massie B, Langelier Y & Brais B (2005). PABPN1 overexpression leads to upregulation of genes encoding nuclear proteins that are sequestered in oculopharyngeal muscular dystrophy nuclear inclusions. *Neurobiol Dis* **18**, 551–567.

Davies JE, Berger Z & Rubinsztein DC (2006). Oculopharyngeal muscular dystrophy: potential therapies for an aggregate-associated disorder. *Int J Biochem Cell Biol* **38**, 1457–1462.

Davies JE, Wang L, Garcia-Oroz L, Cook LJ, Vacher C, O'Donovan DG & Rubinsztein DC (2005). Doxycycline attenuates and delays toxicity of the oculopharyngeal muscular dystrophy mutation in transgenic mice. *Nat Med* **11**, 672–677.

DiFranco M, Quinonez M, Capote J & Vergara J (2009). DNA transfection of mammalian skeletal muscles using in vivo electroporation. *J Vis Exp JoVE* **32**, doi: 10.3791/1520.

Dirksen RT (2002). Bi-directional coupling between dihydropyridine receptors and ryanodine receptors. *Front Biosci J Virtual Libr* **7**, d659–d670.

Dirksen RT (2009). Checking your SOCCs and feet: the molecular mechanisms of Ca2+ entry in skeletal muscle. *J Physiol* **587**, 3139–3147.

Fan X, Dion P, Laganiere J, Brais B & Rouleau GA (2001). Oligomerization of polyalanine expanded PABPN1 facilitates nuclear protein aggregation that is associated with cell death. *Hum Mol Genet* **10**, 2341–2351.

Gach MP, Cherednichenko G, Haarmann C, Lopez JR, Beam KG, Pessah IN, Franzini-Armstrong C & Allen PD (2008). Alpha2delta1 dihydropyridine receptor subunit is a critical element for excitation-coupled calcium entry but not for formation of tetrads in skeletal myotubes. *Biophys J* **94**, 3023–3034.

García J & Beam KG (1994). Measurement of calcium transients and slow calcium current in myotubes. *J Gen Physiol* **103**, 107–123.

Horsley V & Pavlath GK (2004). Forming a multinucleated cell: molecules that regulate myoblast fusion. *Cells Tissues Organs* **176**, 67–78.

Keire P, Shearer A, Shefer G & Yablonka-Reuveni Z (2013). Isolation and culture of skeletal muscle myofibers as a means to analyze satellite cells. *Methods Mol Biol Clifton NJ* **946**, 431–468.

Kim YJ, Noguchi S, Hayashi YK, Tsukahara T, Shimizu T & Arahata K (2001). The product of an oculopharyngeal muscular dystrophy gene, poly(A)-binding protein 2, interacts with SKIP and stimulates muscle-specific gene expression. *Hum Mol Genet* **10**, 1129–1139.

Klein P, Oloko M, Roth F, Montel V, Malerba A, Jarmin S, Gidaro T, Popplewell L, Perie S, Lacau St Guily J, de la Grange P, Antoniou MN, Dickson G, Butler-Browne G, Bastide B, Mouly V & Trollet C (2016). Nuclear poly(A)-binding protein aggregates misplace a pre-mRNA outside of SC35 speckle causing its abnormal splicing. *Nucleic Acids Res* **44**, 10929–10945.

Melzer W, Herrmann-Frank A & Lüttgau HC (1995). The role of Ca2+ ions in excitation-contraction coupling of skeletal muscle fibres. *Biochim Biophys Acta* **1241**, 59–116.

Messaed C & Rouleau GA (2009). Molecular mechanisms underlying polyalanine diseases. *Neurobiol Dis* **34**, 397–405.

Périé S, Mamchaoui K, Mouly V, Blot S, Bouazza B, Thornell L-E, St Guily JL & Butler-Browne G (2006). Premature proliferative arrest of cricopharyngeal myoblasts in oculo-pharyngeal muscular dystrophy: therapeutic perspectives of autologous myoblast transplantation. *Neuromuscul Disord NMD* **16**, 770–781.

Prosser BL, Hernández-Ochoa EO & Schneider MF (2011). S100A1 and calmodulin regulation of ryanodine receptor in striated muscle. *Cell Calcium* **50**, 323–331.

Rebbeck RT, Karunasekara Y, Board PG, Beard NA, Casarotto MG & Dulhunty AF (2014). Skeletal muscle excitation-contraction coupling: who are the dancing partners? *Int J Biochem Cell Biol* **48**, 28–38.

Rios E & Brum G (1987). Involvement of dihydropyridine receptors in excitation-contraction coupling in skeletal muscle. *Nature* **325**, 717–720.

Ríos E, Figueroa L, Manno C, Kraeva N & Riazi S (2015). The couplonopathies: a comparative approach to a class of diseases of skeletal and cardiac muscle. *J Gen Physiol* **145**, 459–474.

Robin G & Allard B (2015). Voltage-gated Ca(2+) influx through L-type channels contributes to sarcoplasmic reticulum Ca(2+) loading in skeletal muscle. *J Physiol* **593**, 4781–4797.

Rodríguez R, Hernández-Hernández O, Magaña JJ, González-Ramírez R, García-López ES & Cisneros B (2015). Altered nuclear structure in myotonic dystrophy type 1-derived fibroblasts. *Mol Biol Rep* **42**, 479–488.

Romberg CF, Beqollari D, Meza U & Bannister RA (2014). RGK protein-mediated impairment of slow depolarization-dependent Ca^{2+} entry into developing myotubes. *Channels Austin Tex* **8**, 243–248.

Royer L, Pouvreau S & Ríos E (2008). Evolution and modulation of intracellular calcium release during long-lasting, depleting depolarization in mouse muscle. *J Physiol* **586**, 4609–4629.

Royer L & Ríos E (2009). Deconstructing calsequestrin. Complex buffering in the calcium store of skeletal muscle. *J Physiol* **587**, 3101–3111.

Tanabe T, Beam KG, Powell JA & Numa S (1988). Restoration of excitation-contraction coupling and slow calcium current in dysgenic muscle by dihydropyridine receptor complementary DNA. *Nature* **336**, 134–139.

Taneja KL, McCurrach M, Schalling M, Housman D & Singer RH (1995). Foci of trinucleotide repeat transcripts in nuclei of myotonic dystrophy cells and tissues. *J Cell Biol* **128**, 995–1002.

Tavanez JP, Calado P, Braga J, Lafarga M & Carmo-Fonseca M (2005). In vivo aggregation properties of the nuclear poly(A)-binding protein PABPN1. *RNA* **11**, 752–762.

Taylor JP, Hardy J & Fischbeck KH (2002). Toxic proteins in neurodegenerative disease. *Science* **296**, 1991–1995.

Vega AV, Ramos-Mondragón R, Calderón-Rivera A, Zarain-Herzberg A & Avila G (2011). Calcitonin gene-related peptide restores disrupted excitation-contraction coupling in myotubes expressing central core disease mutations in RyR1. *J Physiol* **589**, 4649–4669.

Wang Q & Bag J (2006). Ectopic expression of a polyalanine expansion mutant of poly(A)-binding protein N1 in muscle cells in culture inhibits myogenesis. *Biochem Biophys Res Commun* **340**, 815–822.

Wang Y, Xu L, Duan H, Pasek DA, Eu JP & Meissner G (2006). Knocking down type 2 but not type 1 calsequestrin reduces calcium sequestration and release in C2C12 skeletal muscle myotubes. *J Biol Chem* **281**, 15572–15581.

Wang Z-M, Messi ML & Delbono O (1999). Patch-clamp recording of charge movement, Ca^{2+} current, and Ca^{2+} transients in adult skeletal muscle fibers. *Biophys J* **77**, 2709–2716.

Wei-Lapierre L, Carrell EM, Boncompagni S, Protasi F & Dirksen RT (2013). Orai1-dependent calcium entry promotes skeletal muscle growth and limits fatigue. *Nat Commun* **4**, 2805.

Woringer M, Darzacq X & Izeddin I (2014). Geometry of the nucleus: a perspective on gene expression regulation. *Curr Opin Chem Biol* **20**, 112–119.

Yano K & Zarain-Herzberg A (1994). Sarcoplasmic reticulum calsequestrins: structural and functional properties. *Mol Cell Biochem* **135**, 61–70.

Yarotskyy V & Dirksen RT (2012). Temperature and RyR1 regulate the activation rate of store-operated Ca^{2+} entry current in myotubes. *Biophys J* **103**, 202–211.

Additional information

Competing interests

The authors declare that they have no competing interests.

Author contributions

MG-C, AV-V, RR, MGM-J and GA acquired data. MG-C, BC, AZ-H and GA interpreted data. MG-C and GA analysed data. MG-C and GA designed the work. MG-C, AV-V, RR, MGM-J, BC, AZ-H and GA revised the work. Most experiments were performed at the laboratory of GA (Department of Biochemistry, Cinvestav) and the final version of this manuscript was approved by all of the authors. All persons designated as authors qualify for authorship, and all those who qualify for authorship are listed.